Atmos. Chem. Phys., 23, 99–117, 2023
https://doi.org/10.5194/acp-23-99-2023

Atmospheric Chemistry and Physics
Open Access
EGU

Heterogeneity and chemical reactivity of the remote troposphere defined by aircraft measurements – corrected

Hao Guo[1], Clare M. Flynn[2], Michael J. Prather[1], Sarah A. Strode[3], Stephen D. Steenrod[3], Louisa Emmons[4], Forrest Lacey[4,5], Jean-Francois Lamarque[4], Arlene M. Fiore[6], Gus Correa[6], Lee T. Murray[7], Glenn M. Wolfe[3,8], Jason M. St. Clair[3,8], Michelle Kim[9], John Crounse[10], Glenn Diskin[10], Joshua DiGangi[10], Bruce C. Daube[11,12], Roisin Commane[11,12], Kathryn McKain[13,14], Jeff Peischl[14,15], Thomas B. Ryerson[13,15], Chelsea Thompson[13], Thomas F. Hanisco[3], Donald Blake[16], Nicola J. Blake[16], Eric C. Apel[4], Rebecca S. Hornbrook[4], James W. Elkins[14], Eric J. Hintsa[13,14], Fred L. Moore[13,14], and Steven C. Wofsy[11]

[1]Department of Earth System Science, University of California, Irvine, CA 92697, USA
[2]Department of Meteorology, Stockholm University, Stockholm, 106 91, Sweden
[3]Atmospheric Chemistry and Dynamics Laboratory, NASA Goddard Space Flight Center, Greenbelt, MD 20771, USA
[4]Atmospheric Chemistry Observations and Modeling Laboratory, National Center for Atmospheric Research, Boulder, CO 80301, USA
[5]Department of Mechanical Engineering, University of Colorado, Boulder, CO 80309, USA
[6]Department of Earth and Environmental Sciences and Lamont-Doherty Earth Observatory, Columbia University, Palisades, NY 10964, USA
[7]Department of Earth and Environmental Sciences, University of Rochester, Rochester, NY 14611, USA
[8]Joint Center for Earth Systems Technology, University of Maryland, Baltimore County, Baltimore, MD 21228, USA
[9]Department of Geological and Planetary Sciences, California Institute of Technology, Pasadena, CA 91125, USA
[10]Atmospheric Composition, NASA Langley Research Center, Hampton, VA 23666, USA
[11]John A. Paulson School of Engineering and Applied Sciences, Harvard University, Cambridge, MA 02138, USA
[12]Department of Earth and Planetary Sciences, Harvard University, Cambridge, MA 02138, USA
[13]Cooperative Institute for Research in Environmental Sciences, University of Colorado, Boulder, CO 80309, USA
[14]Global Monitoring Division, Earth System Research Laboratory, NOAA, Boulder, CO 80305, USA
[15]Chemical Sciences Division, National Oceanic and Atmospheric Administration Earth System Research Laboratory, Boulder, CO 80305, USA
[16]Department of Chemistry, University of California, Irvine, CA 92697, USA

Correspondence: Hao Guo (haog2@uci.edu) and Michael J. Prather (mprather@uci.edu)

Received: 7 September 2022 – Discussion started: 4 October 2022
Revised: 20 November 2022 – Accepted: 9 December 2022 – Published: 4 January 2023

Abstract. The NASA Atmospheric Tomography (ATom) mission built a photochemical climatology of air parcels based on in situ measurements with the NASA DC-8 aircraft along objectively planned profiling transects through the middle of the Pacific and Atlantic oceans. In this paper we present and analyze a data set of 10 s (2 km) merged and gap-filled observations of the key reactive species driving the chemical budgets of O_3 and CH_4 (O_3, CH_4, CO, H_2O, HCHO, H_2O_2, CH_3OOH, C_2H_6, higher alkanes, alkenes, aromatics, NO_x, HNO_3,

HNO_4, peroxyacetyl nitrate, and other organic nitrates), consisting of 146 494 distinct air parcels from ATom deployments 1 through 4. Six models calculated the O_3 and CH_4 photochemical tendencies from this modeling data stream for ATom 1. We find that 80 %–90 % of the total reactivity lies in the top 50 % of the parcels and 25 %–35 % in the top 10 %, supporting previous model-only studies that tropospheric chemistry is driven by a fraction of all the air. Surprisingly, the probability densities of species and reactivities averaged on a model scale (100 km) differ only slightly from the 2 km ATom 10 s data, indicating that much of the heterogeneity in tropospheric chemistry can be captured with current global chemistry models. Comparing the ATom reactivities over the tropical oceans with climatological statistics from six global chemistry models, we find generally good agreement with the reactivity rates for O_3 and CH_4. Models distinctly underestimate O_3 production below 2 km relative to the mid-troposphere, and this can be traced to lower NO_x levels than observed. Attaching photochemical reactivities to measurements of chemical species allows for a richer, yet more constrained-to-what-matters, set of metrics for model evaluation. This paper presents a corrected version of the paper published under the same authors and title (sans "corrected") as https://doi.org/10.5194/acp-21-13729-2021.

Preface

While continuing our analysis of the NASA Atmospheric Tomography (ATom) data, we found several major mistakes or decision errors. The main conclusions were unchanged except those regarding production of O_3, but most of the numbers and many of the figures changed slightly. A corrigendum to the original 2021 paper was prepared, but the changes were extensive enough so that the *ACP* editors and the authors decided that a completely new paper should be produced and the 2021 paper withdrawn. The errors that were corrected are described in this preface and discussed at most briefly in the paper. First, we found that measurement errors in PAN and HNO_4 were large ($\sim$ 100 ppt), and when this occurred in the lower troposphere, the rapid thermal decomposition released large amounts of NO_x. There is no easy fix for this, and we developed a new protocol (reactivity data stream, RDS*) for computing reactivities by allowing the species to thermally decompose before use in the model, as described below. This fix greatly reduced O_3 production (P-O3) in the lower troposphere. A second NO_x problem involved the propagation of polluted profiles from the Los Angeles basin to gap-filling over the tropical eastern Pacific. This correction resulted in the update of the modeling data stream to version 2b. These NO_x errors cause noticeable changes in reactivities, especially P-O3. Other decision errors led us to decrease the southern latitude extent of the Atlantic and Pacific transects from 54 to 53° S to avoid spurious parcels being included. Also, cosine of latitude weighting was applied to data for all figures and tables. The UCI model now includes all higher alkanes and alkenes in the ATom data as C_3H_8 and C_2H_4, respectively. These last three decision errors had detectable but small impacts.

The most worrisome error was the evolution of the ATom version of the UCI Chemistry Transport Model (CTM) from its use in the MDS-0 (modeling data stream version 0) results shown here to the final calculations with MDS-2 as the UCI2* model in the 2021 paper. The first MDS-0 UCI model was taken directly from the main CTM code line and developed for Prather et al. (2017, 2018) by Xin Zhu (not in the 2021 paper). This model was then further adapted and developed for the 2021 paper and for additional complex sensitivity tests. At this stage (i.e., the UCI2* simulations in the 2021 paper), the results failed several logic tests and were irreproducible. With the decision to withdraw the paper, we returned to the MDS-0 UCI model, and Xin Zhu adapted it to more efficient ATom runs as well as adding several new diagnostics and checks to ascertain the ATom runs were being calculated correctly. As noted in the paper below, we carefully checked the O_3 budget in terms of rates and tendencies, and these are now consistent in the UCIZ (Zhu version) model. Further, the sensitivity coefficients ($\partial \ln R/\partial \ln X$ and $\partial^2 \ln R/\partial \ln X \partial \ln Y$) calculated for a subsequent paper are now closer to theoretical expectations for a quasi-linear system. The UCIZ* model results, calculated with the UCIZ CTM and the RDS* protocol, shown here are our best, revised estimate of the ATom reactivities.

1 Prologue

This paper is based on the methods and results of papers that established an approach for analyzing aircraft measurements, specifically the NASA Atmospheric Tomography Mission (ATom), with global chemistry models. Here we present a brief overview of those papers to help the reader understand the basis for this paper. The first ATom modeling paper ("Global atmospheric chemistry – which air matters", Prather et al., 2017, hence P2017) gathered six global models, both chemistry transport models (CTMs) and chemistry–climate models (CCMs). The models reported a single-day snapshot for mid-August (the time of the first ATom deployment, ATom-1), and these included all species relevant for tropospheric chemistry and the 24 h reactivities. We limited our study to three reactivities (Rs) controlling methane (CH_4) and tropospheric ozone (O_3) using specific reaction rates to define the loss of CH_4 and the production and loss of O_3 in

parts per billion (ppb) per day. The critical photolysis rates (J values) were also reported as 24 h averages.

$$\text{L}-\text{CH4}: \text{CH}_4 + \text{OH} \rightarrow \text{CH}_3 + \text{H}_2\text{O} \quad \text{(R1)}$$

$$\begin{aligned} \text{P}-\text{O3}: &\text{HO}_2 + \text{NO} \rightarrow \text{NO}_2 + \text{RO} && \text{(R2a)}\\ &\text{RO}_2 + \text{NO} \rightarrow \text{NO}_2 + \text{RO}, && \text{(R2b)}\\ &\text{where } \text{NO}_2 + h\nu \rightarrow \text{NO} + \text{O} && \text{(R2c)}\\ &\text{and } \text{O} + \text{O}_2 \rightarrow \text{O}_3 \\ &\text{O}_2 + h\nu \rightarrow \text{O} + \text{O}(x2) && \text{(R2d)} \end{aligned}$$

$$\begin{aligned} \text{L}-\text{O3}: &\text{O}_3 + \text{OH} \rightarrow \text{O}_2 + \text{HO}_2 && \text{(R3a)}\\ &\text{O}_3 + \text{HO}_2 \rightarrow \text{HO} + \text{O}_2 + \text{O}_2 && \text{(R3b)}\\ &\text{O}(^1\text{D}) + \text{H}_2\text{O} \rightarrow \text{OH} + \text{OH} && \text{(R3c)} \end{aligned}$$

$$\text{J}-\text{O1D}: \text{O}_3 + h\nu \rightarrow \text{O}(^1\text{D}) + \text{O}_2 \quad \text{(R4)}$$

$$\text{J}-\text{NO2}: \text{NO}_2 + h\nu \rightarrow \text{NO} + \text{O} \quad \text{(R5)}$$

Models also reported the change in O_3 over 24 h, and these match the P-O3 minus L-O3 values over the Pacific basin (a focus of this study). The models showed a wide range in the three Rs' average profiles across latitudes over the Pacific basin, as well as 2D probability densities (PDs) for key species such as NO_x ($NO + NO_2$) versus HOOH. A large part of the model differences was attributed to the large differences found in chemical composition rather than the calculation of rates from that composition. We found that single transects from a model through the tropical Pacific at different longitudes produced nearly identical 2D PDs, but these PDs were distinctly different across models. This result supported the premise that the ATom PDs would provide a useful metric for global chemistry models.

In P2017, we established a method for running the chemistry modules in the CTMs and CCMs with an imposed chemical composition from aircraft data: the ATom run, or "A run". In the A run, the chemistry of each grid cell does not interact with its neighbors or with externally imposed emission sources. Effectively the CTM/CCM is initialized and run for 24 h without transport, scavenging, or emissions. Aerosol chemistry is also turned off in the A runs. This method allows each parcel to evolve in response to the daily cycle of photolysis in each model and be assigned a 24 h integrated reactivity. The instantaneous reaction rates at the time an air parcel is measured (e.g., near sunset at the end of a flight) do not reflect that parcel's overall contribution to the CH_4 or O_3 budget; a full diel cycle is needed. The A run assumption that parcels do not mix with neighboring air masses is an approximation, and thus for each model we compared the A runs using the model's restart data with a parallel standard 24 h simulation (including transport, scavenging, and emissions). Because the standard grid-cell air moves and mixes, we compared averages over a large region (e.g., tropical Pacific). We find some average biases of order $\pm 10\,\%$ but general agreement. The largest systematic biases in the A runs are caused by buildup of HOOH (no scavenging) and decay of NO_x (no sources). The A runs are relatively easy to code for most CTM/CCMs and allow each model's chemistry module, including photolysis package, to run normally. The A runs do not distinguish between CTMs and CCMs, except that each model will generate/prescribe its own cloud fields and photolysis rates. Our goal is to create a robust understanding of the chemical statistics including the reactivities with which to test and evaluate the free-running CCMs, and thus we do not try to model the specific period of the ATom deployments. Others may use the ATom data with hindcast CTMs to test forecast models, but here we want to build a chemical climatology.

The first hard test of the A runs came with the second ATom modeling paper ("How well can global chemistry models calculate the reactivity of short-lived greenhouse gases in the remote troposphere, knowing the chemical composition", Prather et al., 2018, hence P2018). The UCI CTM simulated an aircraft-like data set of 14 880 air parcels along the International Date Line from a separate high-resolution (0.5°) model. Each parcel is defined by the following core species: H_2O, O_3, NO_x, HNO_3, HNO_4, PAN (peroxyacetyl nitrate), CH_3NO_3, HOOH, CH_3OOH, HCHO, CH_3CHO (acetaldehyde), C_3H_6O (acetone), CO, CH_4, C_2H_6, alkanes (C_3H_8 and higher), C_2H_4, aromatics (benzene, toluene, and xylene), and C_5H_8 (isoprene), plus temperature. Short-lived radicals (e.g., OH, HO_2, and CH_3OO) were initialized at small concentrations and quickly reached daytime values determined by the core species. The six CTM/CCMs overwrote the chemical composition of a restart file, placing each pseudo-observation in a unique grid cell according to its latitude, longitude, and pressure. If another parcel is already in that cell, then it is shifted east–west or north–south to a neighboring model cell. For coarse-resolution models, multiple restart files and A runs were used to avoid large location shifts. CTM/CCMs usually have a locked in 24 h integration step starting at 00:00 UTC that is extremely difficult to modify in order to try to match the local solar time of observation, especially as it changes along aircraft flights. We tested the results with a recoded UCI CTM to start at 12:00 UTC but retain the same clouds fields over the day and found only percentage-level differences between a midnight or noon start.

These A runs averaged over cloud conditions by simulating 5 d in August at least 5 d apart. Assessment of the modeled photolysis rates and comparison with the ATom-measured J values is presented in Hall et al. (2018, hence

H2018). All models agreed that a small fraction of chemically hot air parcels in the synthetic data set controlled most of the total reactivity. Some models had difficulty in implementing the A runs because they overwrote the specified water vapor with the modeled value, but this problem is fixed here. In both P2017 and P2018, the GISS-E2 model stood out with the most unusual chemistry patterns and sometimes illogical correlations. Efforts by a co-author to clarify the GISS results or identify errors in the implementation have not been successful. GISS results are included here for completeness in the set of three papers but are not reconciled. Overall, three models showed remarkable inter-model agreement in the three Rs with less than half of the RMSD (root-mean-square difference) as compared with the other models. UCI also tested the effect of different model years (1997 and 2015 versus reference year 2016), which varies the cloud cover and photolysis rates, and found an inter-year RMSD about half of that of the core model's RMSD. Thus, there is a fundamental uncertainty in this approach due to the inability to specify the cloud/photolysis history seen by a parcel over 24 h, but it is less than the inter-model differences among the most similar models.

2 Introduction

The NASA Atmospheric Tomography (ATom) mission completed a four-season deployment, each deployment flying from the Arctic to Antarctic and back, traveling south through the middle of the Pacific Ocean, across the Southern Ocean, and then north through the Atlantic Ocean, with near-constant profiling of the marine troposphere from 0.2 to 12 km altitude (see Fig. S1 in the Supplement). The DC8 was equipped with in situ instruments that documented the chemical composition and conditions at time intervals ranging from < 1 to about 100 s (Wofsy et al., 2018). ATom measured hundreds of gases and aerosols, providing information on the chemical patterns and reactivity in the vast remote ocean basins, where most of the destruction of tropospheric ozone (O_3) and methane (CH_4) occurs. Reactivity is defined here as in P2017 to include the production and loss of O_3 (P-O3 and L-O3, ppb d^{-1}) and loss of CH_4 (L-CH4, ppb d^{-1}). Here we report on this model-derived product that was proposed for ATom, the daily averaged reaction rates determining the production and loss of O_3 and the loss of CH_4 for 10 s averaged air parcels. We calculate these rates with 3D chemical models that include variations in clouds and photolysis and then assemble the statistical patterns describing the heterogeneity (i.e., high spatial variability) of these rates and the underlying patterns of reactive gases.

Tropospheric O_3 and CH_4 contribute to climate warming and global air pollution (Stocker et al., 2013). Their abundances in the troposphere are controlled largely by tropospheric chemical reactions. Thus, chemistry–climate assessments seeking to understand past global change and make future projections for these greenhouse gases have focused on the average tropospheric rates of production and loss and how these reactivities are distributed in large semi-hemispheric zones throughout the troposphere (Griffiths et al., 2021; Myhre et al., 2014; Naik et al., 2013; Prather et al., 2001; Stevenson, et al., 2006, 2013, 2020; Voulgarakis et al., 2013; Young et al., 2013). The models used in these assessments disagree on these overall CH_4 and O_3 reactivities (a.k.a. the budgets), and resolving the cause of such differences is stymied because of the large number of processes involved and the resulting highly heterogeneous distribution of chemical species that drive the reactions. Simply put, the models use emissions, photochemistry, and meteorological data to generate the distribution of key species such as nitrogen oxides ($NO_x = NO + NO_2$) and hydrogen peroxide (HOOH) (step 1) and then calculate the CH_4 and O_3 reactivities from these species (step 2). There is no single average measurement that can test the verisimilitude of the models. Stratospheric studies such as Douglass et al. (1999) have provided a quantitative basis for testing chemistry and transport and defining model errors, but few of these studies have tackled the problem of modeling the heterogeneity of tropospheric chemistry. The major model differences lie in the first step because when we specify the mix of key chemical species, most models agree on the CH_4 and O_3 chemical budgets (*P2018*). The intent of ATom was to collect an atmospheric sampling of all the key species and the statistics defining their spatial variability and thus that of the reactivities of CH_4 and O_3.

Many studies have explored the ability of chemistry transport models (CTMs) to resolve finer scales such as pollution layers (Eastham and Jacob, 2017; Rastigejev et al., 2010; Tie et al., 2010; Young et al., 2018; Zhuang et al., 2018), but these have not had the chemical observations (statistics) to evaluate model performance. In a great use of chemical statistics, Yu et al. (2016) used 60 s data ($\sim$ 12 km) from the SEAC^{4}RS aircraft mission to compare cumulative probability densities (PDs) of NO_x, O_3, HCHO, and isoprene over the Southeast US with the GEOS-Chem CTM run at different resolutions. They identified clear biases at the high and low ends of the distribution, providing a new test of models based on the statistics rather than mean values. Heald et al. (2011) gathered high-resolution profiling of organic and sulfate aerosols from 17 aircraft missions and calculated statistics (mean, median, and quartiles) but only compared with the modeled means. The HIAPER Pole-to-Pole Observations (HIPPO) aircraft mission (Wofsy, 2011) was a precursor to ATom with regular profiling of the mid-Pacific including high-frequency 10 s sampling that identified the small scales of variability throughout the troposphere. HIPPO measurements were limited in species, lacking O_3, NO_x, and many of the core species needed for reactivity calculations. ATom, with a full suite of reactive species and profiling through the Atlantic basin, provides a wealth of

chemical statistics that challenge the global chemistry models.

One main task here is the assembly of the modeling data stream (MDS), which provides flight-wise continuous 10 s data (air parcels) for the key reactive species. The MDS is based on direct observations and interpolation methods to fill gaps as documented in the Supplement. Using version 0 of the MDS, we have six chemical models calculating the 24 h reactivities, producing a reactivity data stream (RDS version 0) using protocols noted in the Prologue (P2017) and described further in Sect. 3.2. There, we describe the updated modeling protocol RDS* necessary to address measurement noise in PAN and HNO_4, which can be very short-lived. In Sect. 4, we examine the statistics of reactivity over the Atlantic and Pacific oceans, focusing on air parcels with high reactivity; for example, 10 % of the parcels produce 25 %–35 % of total reactivity over the oceans. We compare these ATom-1 statistics, species, and reactivities with August climatologies from six global chemistry models. In one surprising result, ATom-1 shows a more reactive tropical troposphere than found in most models' climatologies associated with higher NO_x levels than in the models. Section 5 concludes that the ATom PDs based on 10s air parcels do provide a valid chemistry metric for global models with 1° resolution. It also presents some examples where ATom measurements and modeling can test the chemical relationships and may address the cause of differences in the O_3 and CH_4 budgets currently seen across the models. With this paper we release the full ATom MDS-2b from all four deployments, along with the updated RDS-2b reactivities from the UCI model.

3 Models and data

3.1 The modeling data stream (MDS)

The ATom mission was designed to collect a multi-species, detailed chemical climatology that documents the spatial patterns of chemical heterogeneity throughout the remote troposphere. Figure S1 maps the 48 research flights, and the Supplement has tables summarizing each flight. We required a complete set of key species in each air parcel to initialize the models that calculate the CH_4 and O_3 reactivities. We choose the key reactive species (H_2O, O_3, CO, CH_4, NO_x, NO_xPSS, HNO_3, HNO_4, PAN, CH_2O, H_2O_2, CH_3OOH, acetone, acetaldehyde, C_2H_6, C_3H_8,*i*-C_4H_{10}, *n*-C_4H_{10}, alkanes, C_2H_4, alkenes, C_2H_2, C_5H_8, benzene, toluene, xylene, CH_3ONO_2, $C_2H_5ONO_2$, $RONO_2$, and CH_3OH) directly from the ATom measurements and then add corollary species or other observational data indicative of industrial or biomass burning pollution or atmospheric processing (HCN, CH_3CN, SF_6, relative humidity, aerosol surface area (four modes), and cloud indicator). We choose 10 s averages for our air parcels as a compromise and because the 10 s merged data are a standard product (Wofsy et al., 2018). A few instruments measure at 1 s intervals, but the variability at this scale is not that different from 10 s averages (Fig. S2). Most of the key species are reported as 10 s values, with some being averaged or sampled at 30 s or longer such as ∼ 90 s for some flask measurements.

Throughout ATom, gaps occur in individual species on a range of timescales due to calibration cycles, sampling rates, or instrument malfunction. The generation of the MDS uses a range of methods to fill these gaps and assigns a flag index to each species and data point to allow users to identify direct measurements and methods used for gap-filling. Where two instruments measure the same species, the MDS selects a primary measurement and identifies which instrument was used with a flag. The methodology and species-specific information on how the current MDS version 2 (MDS-2) is constructed, plus statistics on the 48 research flights and the 146 494 10 s air parcels in MDS-2, are given in the Supplement.

Over the course of this study, several MDS versions were developed and tested, including model-derived RDSs from these versions, some of which are used in this paper. In early ATom science team meetings, there was concern about the accuracy of NO_2 direct measurements when at very low concentrations. A group prepared an estimate for NO_x using the NO and O_3 measurements to calculate a photostationary value for NO_2 and thus NO_x. This PSS-NO_x became the primary NO_x source in version 0 (i.e., MDS-0). With MDS-0, we chose to gap-fill using correlations with CO to estimate the variability of the missing measurement over the gap. The science team then rejected PSS-NO_x as a proxy, and we reverted to the observed $NO + NO_2$ resulting in NO_x values that are 25 % larger on average than in MDS-0 (unweighted mean of 66 vs. 52 ppt). This change affected P-O3 most and L-CH4 least. We then estimated errors in the gap-filling and found that CO had little skill as a proxy for most other species. With MDS-2, we optimized and tested the treatments of gap-filling and lower limit of detection, along with other quality controls. With continued analysis of the unusually reactive eastern Pacific region, we determined that the method of long-gap filling for NO_x resulted in propagation of high NO_x levels from the over-land profiles into the over-water profiles in the tropics. We separated these two set of profiles used for long-gap NO_x filling and created an updated version 2b. This experience points to the importance of having reliable, continuous NO_x measurements. MDS-2b is fully documented in the Supplement.

3.2 The reactivity data stream (RDS)

The concept of using an MDS to initialize 3D global chemistry models and calculate an RDS was developed in the pre-ATom methodology papers (P2017; P2018). In this paper, we use the original six models for their August chemical statistics, and we use five of them plus a box model to calculate the reactivities; see Table 1. The RDS is really a protocol applied to the MDS. It is introduced in the Prologue, and the details can be found in P2018. A model grid cell chosen to be close

Table 1. Chemistry models.

Used for	ID	Model name	Model type	Meteorology	Model grid
clim	GFDL	GFDL-AM3	CCM	NCEP (nudged)	C180 × L48
clim, MDS-0	GISS	GISS-E2.1	CCM	Daily SSTs, nudged to MERRA	2° × 2.5° × 40L
clim, MDS-0	GMI	GMI-CTM	CTM	MERRA	1° × 1.25° × 72L
clim, MDS-0	GC	GEOS-Chem	CTM	MERRA-2	2° × 2.5° × 72L
clim, MDS-0	NCAR	CAM4-Chem	CCM	Nudged to MERRA	0.47° × 0.625° × 52L
clim, MDS-0 & 2b	UCI	UCI-CTM	CTM	ECMWF IFS Cy38r1	T159N80 × L60
MDS-0	F0AM	F0AM	box	MDS + scaled ATom Js	n/a

The descriptions of models used in the paper. The first column denotes if the model's August climatology is used ("clim") and also the MDS versions used. F0AM used chemical mechanism MCMv331 plus J-HNO_4 plus O^1D) + CH_4. For the global models, see P2017, P2017, and H2018. n/a – not applicable.

Table 2. Reactivity statistics for the three large domains (global, Pacific, and Atlantic).

		Models using MDS-0								MDS-2b
Value	Region	F0AM	GC	GISS	GMI	NCAR	UCI	U15	U97	UCIZ*
P-O3, mean, ppb d^{-1}	Global	2.12	2.12	2.57	2.08	2.22	2.38	2.37	2.37	1.23
	Pacific	1.96	2.00	1.99	1.96	2.01	2.17	2.13	2.15	1.11
	Atlantic	1.96	2.12	3.49	2.20	2.44	2.48	2.48	2.49	1.25
L-O3, mean, ppb d^{-1}	Global	1.81	1.63	1.93	1.70	1.76	1.76	1.74	1.75	1.61
	Pacific	1.65	1.51	1.79	1.55	1.52	1.58	1.53	1.56	1.42
	Atlantic	2.15	2.02	2.37	2.17	2.47	2.28	2.28	2.30	2.12
L-CH4, mean, ppb d^{-1}	Global	0.81	0.76	0.43	0.75	0.73	0.79	0.78	0.78	0.61
	Pacific	0.85	0.82	0.40	0.80	0.79	0.82	0.80	0.81	0.63
	Atlantic	0.80	0.78	0.51	0.81	0.86	0.85	0.85	0.85	0.69
P-O3, % of total R in top 10 %	Global	35 %	32 %	31 %	32 %	30 %	34 %	34 %	34 %	33 %
	Pacific	34 %	28 %	28 %	29 %	29 %	30 %	30 %	30 %	27 %
	Atlantic	24 %	25 %	24 %	26 %	24 %	27 %	27 %	28 %	27 %
L-O3, % of total R in top 10 %	Global	35 %	35 %	33 %	35 %	36 %	36 %	36 %	36 %	36 %
	Pacific	33 %	32 %	29 %	32 %	31 %	32 %	32 %	32 %	32 %
	Atlantic	28 %	30 %	29 %	30 %	34 %	30 %	30 %	30 %	29 %
L-CH4, % of total R in top 10 %	Global	33 %	30 %	27 %	31 %	31 %	32 %	32 %	32 %	30 %
	Pacific	32 %	28 %	26 %	29 %	29 %	29 %	29 %	29 %	27 %
	Atlantic	27 %	25 %	21 %	26 %	27 %	27 %	27 %	27 %	25 %

Global includes all ATom-1 parcels, Pacific considers all measurements over the Pacific Ocean from 53° S to 60° N, and Atlantic uses parcels from 53° S to 60° N over the Atlantic Ocean. All parcels are weighted inversely by the number of parcels in each 10° latitude by 100 hPa bin and by cosine(latitude). Results from MDS-0 are shown because we have results from six models. Results from the updated MDS-2b are shown (UCIZ*) using the using the current UCI CTM model UCIZ and the RDS* protocol that preprocesses the MDS-2b initializations with a 24 h decay of HNO4 and PAN according to their local thermal decomposition frequencies; see text. See additional statistics in Table S8.

to the measured parcel is initialized with all the core reactive species needed for a regular chemistry simulation. The model is then integrated over 24 h without transport or mixing, without scavenging, and without emissions. Each global model uses its own varying cloud fields for the period to calculate photolysis rates, but the F0AM box model simply takes the instant J values as measured on the flight and applies a diurnal scaling. We initialize with the core species and let the radicals (OH, HO_2, and RO_2) come quickly into photochemical balance. The 24 h integration is not overly sensitive to the start time of the integration, and thus models do not have to synchronize with the local time of observation (see P2018's Fig. S8 and Table S8).

The initial ATom-1 reactivities came from MDS-0 and six of the models in Table 1. Although these RDS-0 model results are now out of date because of the move to MDS-2b, they provide critical information on how models agree, or disagree, in calculating the RDS using the ATom protocol. Thus we include them here as a cross-model comparison. Given the excellent agreement at the parcel level using three models (GC, GMI, and UCI), and with a desire to avoid wasting the community's time, we continued the analysis of

Table 3. Cross-model rms differences (RMSDs as a percentage of the mean) for the three reactivities using MDS-0.

P-O3	F0AM	GC	GISS	GMI	NCAR	UCI
F0AM		48 %	95 %	45 %	55 %	42 %
GC	48 %		78 %	**26 %**	42 %	**32 %**
GISS	95 %	78 %		81 %	72 %	75 %
GMI	45 %	**26 %**	81 %		40 %	**35 %**
NCAR	55 %	42 %	72 %	40 %		42 %
UCI	42 %	**32 %**	75 %	**35 %**	42 %	*(10 %)*
L-O3						
F0AM		40 %	44 %	43 %	76 %	38 %
GC	40 %		33 %	**25 %**	60 %	**24 %**
GISS	44 %	33 %		36 %	66 %	30 %
GMI	43 %	**25 %**	36 %		62 %	**28 %**
NCAR	76 %	60 %	66 %	62 %		60 %
UCI	38 %	**24 %**	30 %	**28 %**	60 %	*(11 %)*
L-CH4						
F0AM		47 %	136 %	48 %	82 %	45 %
GC	47 %		111 %	**20 %**	60 %	**27 %**
GISS	136 %	111 %		114 %	110 %	121 %
GMI	48 %	**20 %**	114 %		57 %	**30 %**
NCAR	82 %	60 %	110 %	57 %		68 %
UCI	45 %	**27 %**	121 %	**30 %**	68 %	*(14 %)*

Matrices are symmetric. Calculated with the 31 376 MDS-0 unweighted ATom-1 parcels using the standard RDS protocol. F0AM lacks 5510 of these parcels because there are no reported J values. UCI shows RMSD between years 2016 (default) and 1997 as the value in parentheses on the diagonal. The unweighted mean R from three core models (GC, GMI, and UCI) are P-O3 = 1.97, L-O3 = 1.50, and L-CH4 = 0.66 (all ppb d^{-1}). The three core-model RMSDs with respect to one another are less than 36 % and given in bold.

MDS-2b with just our local UCI CTM. This decision may need to be revisited.

Statistics for the three reactivities for six models using MDS-0 are given in Tables 2 and S8 for three domains: global (all points), Pacific (oceanic data from 53° S to 60° N), and Atlantic (same constraints as Pacific). The statistics try to achieve equal latitude-by-pressure sampling by weighting each ATom parcel inversely according to the number of parcels in each 10° latitude by 100 hPa bin, and each point is also cosine (latitude)-weighted. We calculate the means and medians plus the percent of total reactivity in the top 10 % of the weighted parcels (Table 2) and also the mean reactivity of the top 10 %, percent of total reactivity in the top 50 %, 10 %, and 3 %, plus the mean J values (Table S8).

These six-model version 0 statistics are shown alongside the version 2b results using the current UCIZ model but with a new protocol designated RDS*. While investigating sensitivities in the RDS, we found an inconsistency between the reported concentrations of both pernitric acid (HNO_4) and peroxyacetyl nitrate (PAN) with respect to the chemical kinetics used in the models. High concentrations (100 ppt, attributed to instrument noise) were reported under conditions where the thermal decomposition frequency was > 0.4 per hour in the lower troposphere (> 253 K for HNO_4 and > 291 K for PAN). Thus, these species instantly become NO_x. While these measurements are clearly spurious, there is no easy fix. We developed a new protocol, RDS*, that allows both species to decay for 24 h using their local thermal decomposition rate before being used in the model. This protocol avoids much of the fast thermal release of NO_x in the lower atmosphere during the first 24 h of the RDS calculation but does not affect the release of NO_x from photolysis or OH reactions in the upper troposphere where thermal decomposition is inconsequential. It is possible that some of the high concentrations of HNO_4 and PAN in the lower troposphere are real and that we are missing this large source of NO_x with the RDS* protocol, but we find no obvious sources of these species in the remote oceanic regions that would produce enough to match the thermal loss. Both this problem and its solution do not affect the initial NO_x values.

We present the RDS-2b reactivities calculated under the RDS* protocol with the UCI CTM developed by Xin Zhu for P2017 and P2018 (designated UCIZ*) as our best results in the final column of Tables 2 and S8. We added diagnostics that give us confidence in our O_3 reactivities: the approximate P-O3 and L-O3 based on the limited Reactions (rates 2a, b, and d and 3a, b, and c above) actually predict the calculated 24 h O_3 tendency; see Fig. S6. Considering the ocean basin observations only, P − L (production minus loss) ranges from -12 to $+15$ ppb d^{-1}. The mean error in P–L is about -0.01 ppb d^{-1}, and the root-mean-squared error is about 0.04 ppb d^{-1}, convincing us that we have correctly diagnosed the P-O3 and L-O3 terms. Following the practice of the GMI model, we also record the initial and 24 h abundances of all the ATom species to check that nothing unusual altered the species abundance in each cell over the 24 h.

3.3 Inter-model differences

Variations in reactivities due to clouds are an irreducible source of uncertainty: predicting the cloud-driven photolysis rates that a shearing air parcel will experience over 24 h is not possible here. The protocol uses 5 separated 24 h days to average over synoptically varying cloud conditions. The standard deviation (σ) of the 5 d, as a percentage of the 5 d mean, is averaged over all parcels and shown in Table S9 for the five global models. Three central models (GC, GMI, and UCI) show 9 %–10 % σ (Js) values and similar σ (Rs) values as expected if the variation in J values is driving the reactivities. Two models (GISS and NCAR) have 12 %–17 % σ (Js), which might be explained by more opaque clouds, but the amplified $\sigma(R)$ values (14 %–32 %) are inexplicable. This discrepancy needs to be resolved before using these two models for ATom RDS analysis.

Inter-model differences are shown in the parcel-by-parcel root-mean-square (rms) differences for RDS-0 in Table 3. Even when models adopt standard kinetic rates and cross sections (i.e., Burkholder et al., 2015), the number of species and chemical mechanisms included, as well as the treatment of families of similar species or intermediate short-lived reac-

Table 4. ATom data files used here.

Primary aircraft data	Formatting and content	Comments
(a) Mor.all.at1234.2020-05-27.tbl (b) Mor.WAS.all.at1234.2020-05-27.tbl (c) Mor.TOGA.all.at1234.2020-05-27.tbl All from Wofsy et al. (2018).	(a) 149 133 records × 675 csv columns, 10 s merges of flight data plus chemistry & environmental measurements (b) 6991 records × 729 csv columns, 30–120 s intervals to fill flasks (c) 12 168 records × 727 csv columns, 35 s intervals of instrument	Core source of ATom measurements. Irregular and difficult formatting, extremely long asci records, large negative integers or "NA" for some non-data.
Modeling data stream (MDS-2b)		
(a) ATom_MDS2b.nc	(a) netCDF file containing regularly spaced 10 s observations for ATom-1 (32 383 records), ATom-2 (33 424 records), ATom-3 (40 176 records), and ATom-4 (40 511 records), 146 494 in total. Includes physical flight data (11), chemical data (39), miscellaneous data including corrected HNO4 and PAN (6), and flag data (50).	Regular formatting; all data gap-filled with flags to identify the method and extent of filling; NaN's only for flight 46; for use in modeling of the chemistry and related statistics from the ATom 10 s data.
Reactivity data stream (RDS-2b)		
(a) ATom_RDS2b.nc	(a) netCDF file containing regularly spaced reactivities for 10 s parcels from ATom-1234 (146 494 in total). Includes latitude, longitude, and pressure of model grid cell used in the calculation. Includes P-O3, L-O3, L-CH4, L-CO, and J-O1D, plus dO_3/dt = net O_3 change over 24 h. Reactivities are given for 5 d separated by 5 d in the middle of each deployment, plus the 5 d mean.	Results from newest UCI CTM version (UCIZ) run with RDS* protocol (PAN and HNO_4 decay) and using MDS-2b. NaN's only for flight 46.

tion products, varies across models. For example, UCI considers about 32 reactive gases, whereas GC and GMI have over 100, and F0AM has more than 600. The other major difference across models is photolysis, with models having different cloud data and different methods for calculating photolysis rates in cloudy atmospheres (H2018). The three central models (GC, GMI, and UCI) in terms of their 5 d variability (Table S9) are also most closely alike in these statistics, with rms = 20 %–30 % for L-CH4 up to 26 %–35 % for P-O3. These rms values appear to be about as close as any two models can get. The intra-model rms for different years (UCI 2016 versus 1997) is 10 %–13 % and shows that we are seeing basic differences in the chemical models across GC, GMI, and UCI. F0AM is the next closest to these central models, but it will inherently have a larger rms because it is a 1 d calculation and not a 5 d average. NCAR's rms is consistently higher and likely related to what is seen in the 5 d σ values in Table S9. GISS is clearly different from all the others (L-CH4 rms > 100 %, while L-O3 rms < 66 %).

4 Results

Our analysis of the reactivities uses the six-model RDS-0 results to examine the consistency in calculating the Rs across models. Thereafter, we rely on the similar results from the three central models (GC, GMI, and UCI) to justify use of UCIZ* with MDS-2b as our best estimate for ATom reactivities. The uncertainty in this estimate can be approximated by the inter-model spread of the central models as discussed above. When evaluating the model climatologies for chemical species, we use MDS-2b. A summary of the key data files used here, as well as their sources and contents, is given in Table 4.

4.1 Probability densities of the reactivities

The reactivities for three large domains (global, Pacific, and Atlantic) from the six-model RDS-0 are summarized in Tables 2 and S8. Sorted PDs for the three Rs and Pacific and Atlantic Ocean basins are plotted in Fig. 1 and show the importance of the most reactive "hot" parcels with deeply convex curves and the sharp upturn in R values above 0.9 cumulative weight (top 10 %). Both basins show a similar emphasis on the most reactive hot parcels: 80 %–90 % of total R is in the top 50 % of the parcels, 25 %–35 % is in the top 10 %, and about 10 %–14 % is in the top 3 %. The corollary is that the bottom 50 % parcels control only 10 %–20 % of the to-

tal reactivity, which is why the median is less than the mean (except for P-O3 in the Atlantic).

The enhancement factor for the top 50 % L-CH4 parcels is 2.0 (84 % of reactivity in 42 % of mass) given that our 53° S–60° N transects cover 83 % of the air mass below 200 hPa and assuming that L-CH4 is negligible poleward of these transects. This enhancement factor is a large-scale feature because the tropical lower troposphere, being warm and wet with high sun, dominates the budget. It is seen in previous model intercomparisons that calculate budgets in large tropospheric blocks like Voulgarakis et al. (2013) with 63 % of L-CH4 in 31 % of the air mass (500 hPa–surface, 30° S–30° N). The impact of the extremely hot parcels and the heterogeneity seen in the ATom 10 s parcels is evident in the steep slopes above the 90th percentile, yielding enhancement factors of 3 to 4.

Each R value and each ocean has a unique shape; for example L-O3 in the Atlantic is almost two straight lines breaking at the 50th percentile. In Fig. 1 the agreement across all models (except GISS) is clear, indicating that the conclusion in *P2018* (i.e., that most global chemistry models agree on the O_3 and CH_4 budgets if given the chemical composition) also holds for the ATom-measured chemical composition. Comparing the dashed brown (UCI, RDS-0) and black (UCIZ, RDS*-2) lines, we find that the shift from MDS-0 to MDS-2b plus the new RDS* (HNO_4 + PAN) protocol produces large reductions in P-O3 for all cumulative weights and small reductions in L-CH4 for the upper 5th percentile. We conclude that accurate modeling of chemical composition of the 80th and greater percentiles is important but that modest errors in the lowest 50th percentile are inconsequential; effectively, some parcels matter more than others (P2017).

How well does this ATom analysis work as a model intercomparison project? Overall, we find that most models give similar results when presented with the ATom-1 MDS. The broad agreement of the cumulative reactive PDs across a range of model formulations using differing levels of chemical complexity shows this approach is robust. The different protocols for calculating reactivities as well as the uncertainty in cloud fields appear to have a small impact on the shape of the cumulative PDs but are informative regarding the minimum structural uncertainty in estimating the 24 h reactivity of a well-measured air parcel.

4.2 Spatial heterogeneity of tropospheric chemistry

A critical unknown for tropospheric chemistry modeling is what resolution is needed to correctly calculate the budgets of key gases. A similar question was addressed in Yu et al. (2016) for the isoprene oxidation pathways using a model with variable resolution (500, 250, and 30 km) compared to aircraft measurements; see also ship plume chemistry in Charlton-Perez et al. (2009). ATom's 10 s air parcels measure 2 km (horizontal) by 80 m (vertical) during most profiles. There are obviously some chemical structures below the 10 s air parcels. Only some ATom measurements are archived at 1 Hz, and we examine a test case using 1 s data for O_3 and H_2O for a mid-ocean descent between Anchorage and Kona in Fig. S2a. Some of the 1 s (200 m by 8 m) variability is clearly lost with 10 s averaging, but 10 s averaging preserves most of the variability. Lines in Fig. S2 demark 400 m in altitude, and most of the variability occurs on this larger, model-resolved scale. Figure S2b shows the 10 s reactivities during that descent and also indicates that much of the variability occurs at 400 m vertical scales. A more quantitative example using all the tropical ATom reactivities is shown in comparisons with probability densities below (Fig. 5).

How important is it for the models to represent the extremes of reactivity? While the sorted reactivity curves (Fig. 1, Tables 2 and S8) continue to steepen from the 90th to 97th percentile, the slope does not change that much. Thus we can estimate the 99th+ percentile contributes < 5 % of the total reactivity. Thus, if our model misses the top 1 % of reactive air parcels (e.g., due to the inability to simulate intensely reactive thin pollution layers) then we miss at most 5 % of the total reactivity. This finding is new and encouraging, and it needs to be verified with the ATom-2, 3, and 4 data.

The spatial structures and variability of reactivity as sampled by the ATom tropical transects (central Pacific, eastern Pacific, and Atlantic) are presented as nine panels in Fig. 2. Here, the UCIZ RDS*-2 reactivities are averaged and plotted in 1° latitude by 200 m thick cells, comparable to some global models (e.g., GMI, NCAR, and UCI). We separate the eastern Pacific (121° W, research flight (RF) 1) from the central Pacific (RFs 3, 4, and 5) because we are looking for contiguous latitude-by-pressure structures.

In the central Pacific (Fig. 2a, d, g), highly reactive (hot) P-O3 parcels (> 6 ppb d^{-1}) occur in larger, connected air masses at latitudes 20–22° N and pressure altitudes 2–3 km and in more scattered parcels (> 3 ppb d^{-1}) below 5 km down to 20° S. High L-O3 and L-CH4 coincide with this 20–22° N air mass and also with some high P-O3 at lower latitudes. This pattern of overlapping extremes in all three Rs is surprising because the models' mid-Pacific climatologies show a separation between regions of high L-O3 (lower–middle troposphere) and high P-O3 (upper troposphere, as seen in P2017's Fig. 3). The obvious explanation is that the models leave most of the lightning-produced NO_x in the upper troposphere. The ATom profiling seems to catch reactive regions in adjacent profiles separate by a few hundred kilometers, scales easily resolvable with 3D models.

In the eastern Pacific (Fig. 2b, e, h), the overlap of outbound and return profiles enhances the spatial sampling over the 10 h flight. The region of very large L-O3 (> 5 ppb d^{-1}) is extensive, beginning at 5–6 km at 10° N and broadening to 2–8 km at 28° N. The region of L-CH4 is similar, but loss at the upper altitudes of this air mass is attenuated because of the temperature dependence of L-CH4 and possibly because of differing OH : HO_2 ratios with altitude. Large P-O3

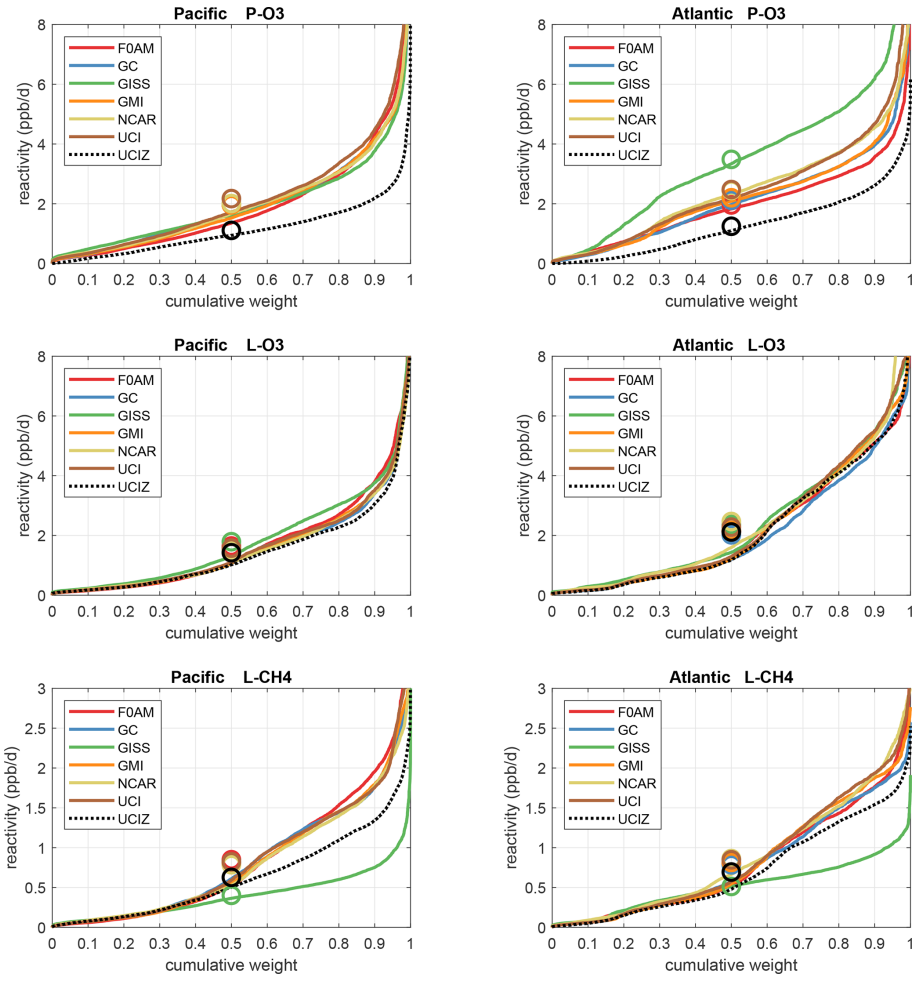

Figure 1. Sorted reactivities (P-O3, L-O3, and L-CH4, in ppb d^{-1}; three successive rows) for the Pacific and Atlantic domains (53° S–60° N, two columns) of ATom-1. Each parcel is weighted, including cosine (latitude); see text. Results from six models using MDS-0 and the standard RDS protocol are shown with colored lines; the updated UCIZ CTM using MDS-2b with the RDS* protocol (HNO_4 and PAN damping) is shown as a dashed black line. The mean value for each model is shown with an open circle plotted at the 50th percentile. (Flipped about the axes, this is a cumulative probability density function.)

(> 3 ppb d^{-1}) occurs only in the center of this highly reactive L-O3/L-CH4 region, suggesting that NO_x is not as evenly distributed as HO_x is. Highly reactive (hot) P-O3 parcels (> 4 ppb d^{-1}) occur only in the upper troposphere (8–12 km) and only in the sub-tropics. ATom-1 RF1 (29 July 2016) occurred during the North American Monsoon when there was easterly flow off Mexico; thus the high reactivity of this large air mass indicates that continental deep convection with lightning NO_x is a source of high reactivity for both O_3 and CH_4.

In the Atlantic (Fig. 2c, f, i), we also see similar air masses through successive profiles, particularly in the northern tropics. The Atlantic P-O3 shows high-altitude reactivity similar to the eastern Pacific. Likewise, the large values of L-O3 and L-CH4 match the eastern Pacific and not the central Pacific. Unlike either Pacific transect, the Atlantic L-O3 and L-CH4 show some high reactivity below 1 km altitude. Overall, the ATom-1 profiling clearly identifies extended air masses of high L-O3 and L-CH4 extending over 2–5 km in altitude and 10° of latitude. The high P-O3 regions tend to be much more heterogeneous with greatly reduced spatial extent, likely of recent convective origin as for the eastern Pacific.

Overall, the extensive ATom profiling identifies a heterogeneous mix of chemical composition in the tropical Atlantic and Pacific, with a large range of reactivities. What is important for those trying to model tropospheric chemistry is that the spatial scales of variability seen in Fig. 2 should be within the capability of modern global models.

4.3 Testing model climatologies

The ATom data set provides a unique opportunity to test CTMs and CCMs in a climatological sense. In this section, we compare ATom-1 data and the six models' chemical

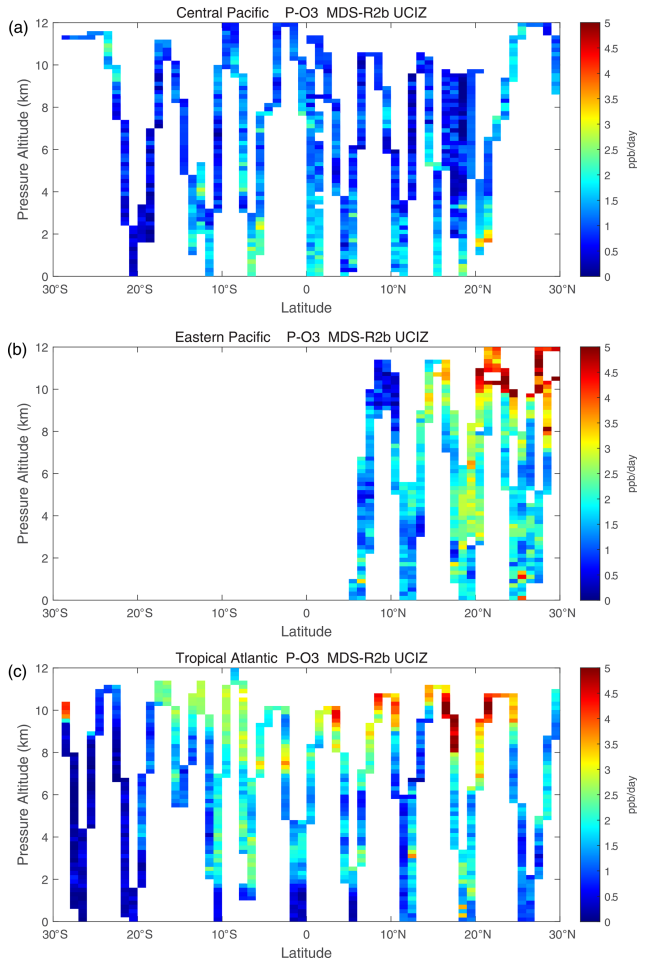

Figure 2.

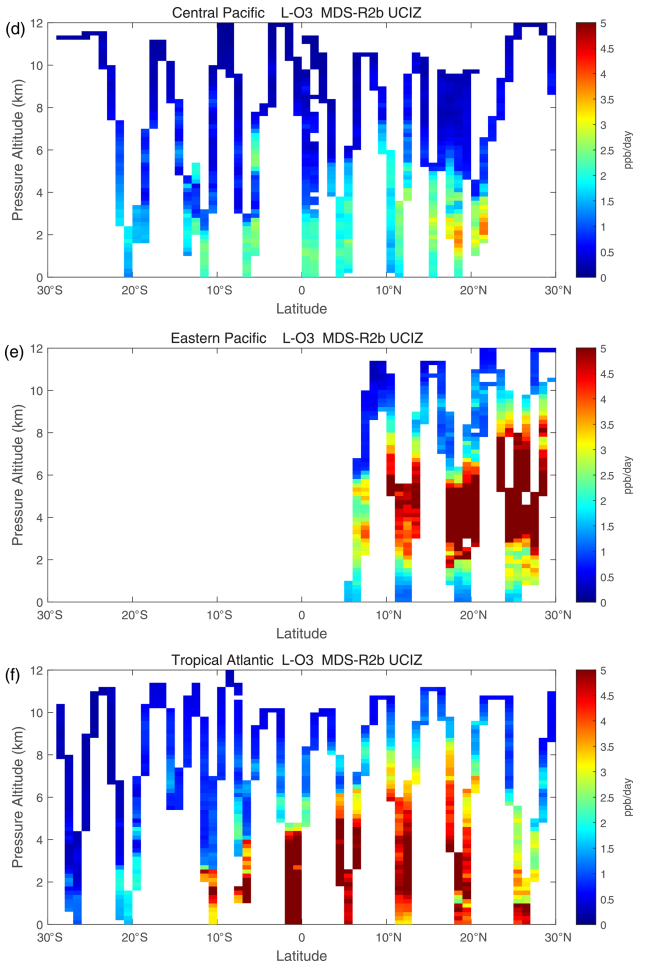

Figure 2.

statistics for mid-August used in P2017. The ATom profiles cannot be easily compared point by point with CCMs, and we use statistical measures of the three reactivities in the three tropical basins: mean profiles in Fig. 3 and PDs in Fig. 5.

4.3.1 Profiles

For P-O3 profiles (top row, Fig. 3), the agreement between models and measurements is passable except for the 0–2 km region in both the central and eastern Pacific, where the models fail to predict the observed 2 ppb d^{-1} O_3 production. In the central Pacific at 3–12 km, ATom-1 results agree with models, showing ozone production of about 1 ppb d^{-1}. In the eastern Pacific and Atlantic at 3–12 km, ATom-1 results also agree with models but at a higher ozone production of about 2 ppb d^{-1}. This pattern indicates that in the central Pacific, the $NO_x + HO_x$ combination that produces ozone is suppressed below 2 km in all the models. In the upper troposphere, 10–12 km, of the eastern Pacific and Atlantic, ATom P-O3 values show a jump to 3 ppb d^{-1}, which is only partly reproduced in the models. We take this pattern as evidence for lightning NO_x production and export over the adjacent continents.

For L-O3 (middle row, Fig. 3) in the central Pacific, ATom-1 results match the throughout the 0–12 km range (except GISS). Moving to the eastern Pacific and Atlantic, most models show a mid-level peak above 2 km, while ATom-1 shows an even larger peak for L-O3, especially in the eastern Pacific at 3–6 km where L-O3 > 4 ppb d^{-1}. This mid-tropospheric peak is evident in the curtain plots of Fig. 2 and likely due to easterly mid-tropospheric flow from convection over Mexico at that specific time (29 July 2016). Similarly, the ATom reactivity at 1–3 km in the Atlantic is associated with biomass burning in Africa and was measured in other trace species. Thus, in terms of L-O3, the ATom–model differences may be due to specific meteorological conditions, and this could be tested with CTMs using 2016 meteorology and wildfires.

For L-CH4 (bottom row, Fig. 3), the ATom–model patterns are similar to L-O3, including the large ATom-only losses (> 1.5 ppb d^{-1} over 3–6 km) in the eastern Pacific but with higher reactivities occurring at slightly lower altitudes because of the large negative temperature dependence of Reac-

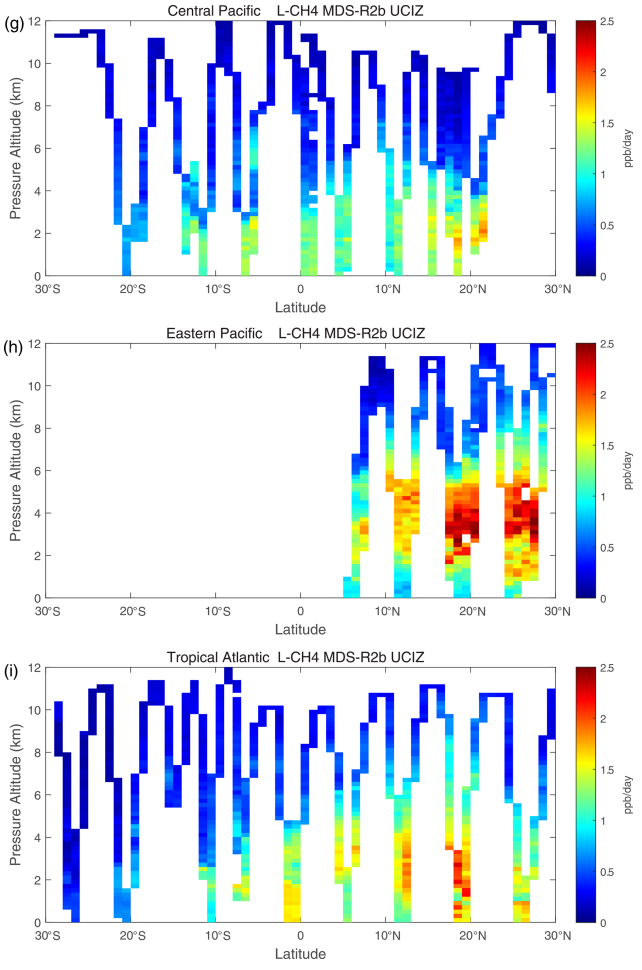

Figure 2. Curtain plots for P-O3 (0–5 ppb d^{-1}; panels **a, b, c**), L-O3 (0–5 ppb d^{-1}; panels **d, e, f**), and L-CH4 (0–2.5 ppb d^{-1}; panels **g, h, i**) showing the profiling of ATom-1 flights in the central Pacific (RF 3, 4 and 5; panels **a, d, g**), eastern Pacific (RF 1; panels **b, e, h**), and Atlantic (RF 7, 8, and 9; panels **c, f, i**). Reactivities are calculated with the current UCIZ CTM model using MDS-2b and the RDS* protocol; see text. The 10 s air parcels are averaged into 1° latitude and 200 m altitude bins.

tion (1). L-O3 is dominated by O(1D) and HO_2 loss, while L-CH4 is limited to OH loss. Overall, there is clear evidence that the Atlantic and Pacific have very different chemical mixtures controlling the reactivities and that convection over land (monsoon or biomass burning) creates air masses that are still highly reactive a day or so later.

4.3.2 Key species

The deficit in modeled P-O3 in the central and eastern Pacific at 0–2 km altitude points to a NO_x deficiency in the models, and this becomes obvious in the comparison of the PD histograms for NO_x shown in Fig. 4. Over 0–12 km (first row), ATom has a reduced frequency of parcels with 1–10 ppt and a corresponding increase in parcels with 20-60 ppt; this discrepancy is amplified in the lower troposphere, 0–4 km (second row). The obvious source of this oceanic NO_x is lightning since oceanic sources of organonitrates or other nitrate species measured on ATom could not supply this amount. The ATom statistics indicate such a lightning source must be mixed down into the boundary layer. In the eastern Pacific and Atlantic, the full troposphere PD more closely matches the models, including a bump in 100–300 ppt NO_x which is probably direct outflow from very deep convection with lightning over the neighboring continents. Overall, the models appear to be missing significant NO_x sources in all three regions below 4 km.

In Fig. 4, we also look at the histograms for the key HO_x-related species HOOH (third row) and HCHO (fourth row). For these species, the ATom–model agreement is generally good. If anything, the models tend to have too much HOOH. ATom shows systematically large occurrences of low HOOH (50–200 ppt, especially in the central Pacific), indicating, perhaps, that convective or cloud scavenging of HOOH is more effective than is modeled. HCHO shows reasonable agreement in the Atlantic, but in both the central and eastern Pacific, the modeled low end (< 40 ppt) is simply not seen in the ATom data. Also, the models are missing a strong HCHO peak at 300 ppt in the eastern Pacific, probably convection-related, specific to that time period. Thus, in terms of these HO_x precursors, the model climatologies appear to be at least as reactive as the ATom data.

While the ATom-1 data in Fig. 4 are limited to single transects, the model NO_x discrepancies apply across the three tropical regions, and the simple chemical statistics for these flights alone are probably enough to identify measurement–model discrepancies. For the HO_x-related species, the models match the first-order statistics from ATom. In terms of using ATom statistics as a model metric, it is encouraging that where some individual models tend to deviate from their peers, they also deviate from the ATom-1 PDs.

4.3.3 Probability densities

Mean profiles do not reflect the heterogeneity seen in Fig. 2, and so we also examine the PDs of the tropical reactivities (Fig. 5). The model PDs (colored lines connecting open circles at the center of each bin) are calculated from the 1 d statistics for mid-August (P2017) using the model blocks shown in Fig. S1. The model grid cells are weighted by air mass and cosine(latitude) and limited to pressures greater than 200 hPa. The ATom PDs (black lines connecting black open circles) are calculated from the 10 s data weighted by (but not averaged over) the number of points in each 10° latitude by 200 hPa pressure bin and then also by cosine (latitude) to compare with the models. In addition, a PD was calculated from the 1° by 200 m average grid-cell values in Fig. 2 (black Xs), and this is also cosine (latitude)-weighted. To check if the high reactivities in the eastern Pacific affected the whole Pacific PD, a separate PD using only central Pacific

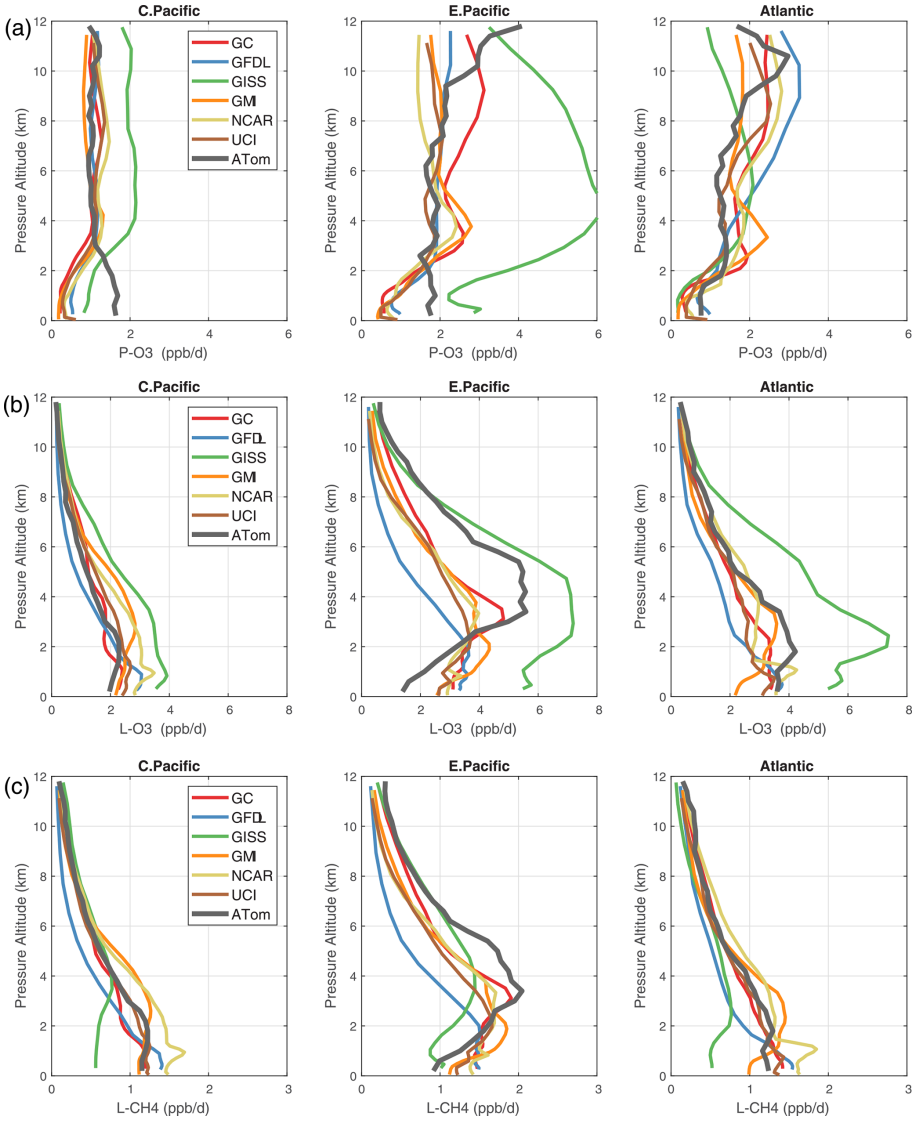

Figure 3. Mean altitude profiles of reactivity (rows: P-O3, L-O3, L-CH4 in ppb d^{-1}) in three domains (columns: C. Pacific, 30° S–30° N by 180–210° E; E. Pacific, 0–30° N by 230–250° E; Atlantic, 30° S–30° N by 326–343° E; ranges are the model blocks). Air parcels are cosine (latitude)-weighted. ATom-1 (gray) results are from Fig. 2, while model results are taken from the August climatologies in Prather et al. (2017).

10 s data was calculated (gray lines connecting open gray circles). The mean reactivities (ppb d^{-1}) from the models and ATom are given in the legend; note that the model values are based on the August climatologies (P2017) and not the MDS-0 values in the table. The "ATom" legend values are the same as in Table 2. The PD binning is shown by the open circles, and occurrences of off-scale reactivities are included in the last point.

For the Pacific (eastern + central, left columns, Fig. 5), the modeled PD climatologies are similar for each of the reactivities (except GISS), and there is fairly good agreement with the ATom-1 PDs. For the Atlantic (right columns, Fig. 5), the models show a larger spread, presumably due to the differing influence of pollution from neighboring continents. The ATom-1 Atlantic PDs also show slightly larger disagreement with the models (e.g., the maximum in P-O3 at 1–2 ppb d^{-1} and minimum in L-O3 at 2–3 ppb d^{-1}) and the notably higher frequency of hot spots with L-O3 $>$ 5 ppb d^{-1}. The influence of the extreme eastern Pacific reactivities is seen in the statistics generated from the central Pacific values only (CPac; gray circles); e.g., the mean value for L-O3 drops from 1.42 to 1.17 ppb d^{-1}.

The ability to test a model's reactivity statistics with the ATom 10 s data is not obvious, but the PDs based on 1° latitude by 200 m altitude cells (the black Xs) are remarkably close to the PDs based on 2 km (horizontal) by 80 m (vertical)

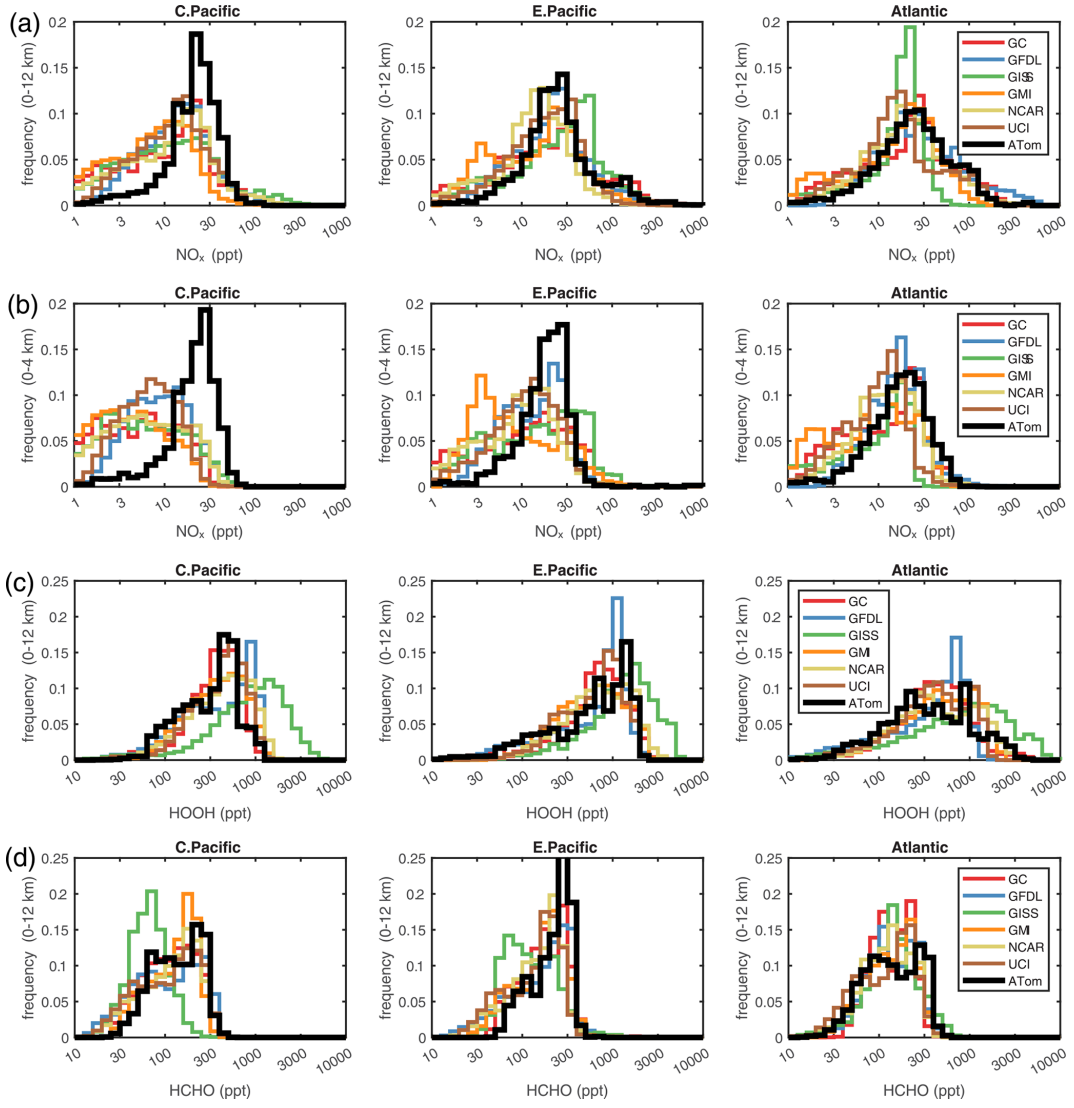

Figure 4. Histograms of probability densities (PDs) of NO_X (0–12 km, **a**), NO_X (0–4 km, **b**), HOOH (0–12 km, **c**), and HCHO (0–12 km, **d**) for the three tropical regions (central Pacific, eastern Pacific, and Atlantic). The ATom-1 data are plotted on top of the six global chemistry models' results for a day in mid-August and sampled as described in Fig. 3.

10 s parcels. With the coarser resolution, we see a slight shift of points from the ends of the PD to the middle as expected, but we find, once again, that the loss in high-frequency, below-model grid-cell resolution is not great. Both ATom-derived PDs more closely resemble each other than any model PD. Thus, current global chemistry models with resolutions of about 100 km by 400 m should be able to capture much of the wide range of chemical heterogeneity in the atmosphere, which for the oceanic transects is, we believe, adequately resolved by the 10 s ATom measurements. Perhaps more surprising, given the different mean profiles in Fig. 3, is that the five model PDs in Fig. 5 look very much alike.

5 Discussion and path forward

5.1 Major findings

This paper opens a door for what the community can do with the ATom measurements and the derived products. ATom's mix of key species allows us to calculate the reactivity of the air parcels and hopefully may become standard for tropospheric chemistry campaigns. We find that the reactivity of the troposphere with respect to O_3 and CH_4 is dominated by a fraction of the air parcels but not by so small and infrequent a fraction as to challenge the ability of current CTMs to simulate these observations and thus be used to study the oxidation budgets. In comparing ATom results with modeled climatologies, we find a systematic ATom–model difference:

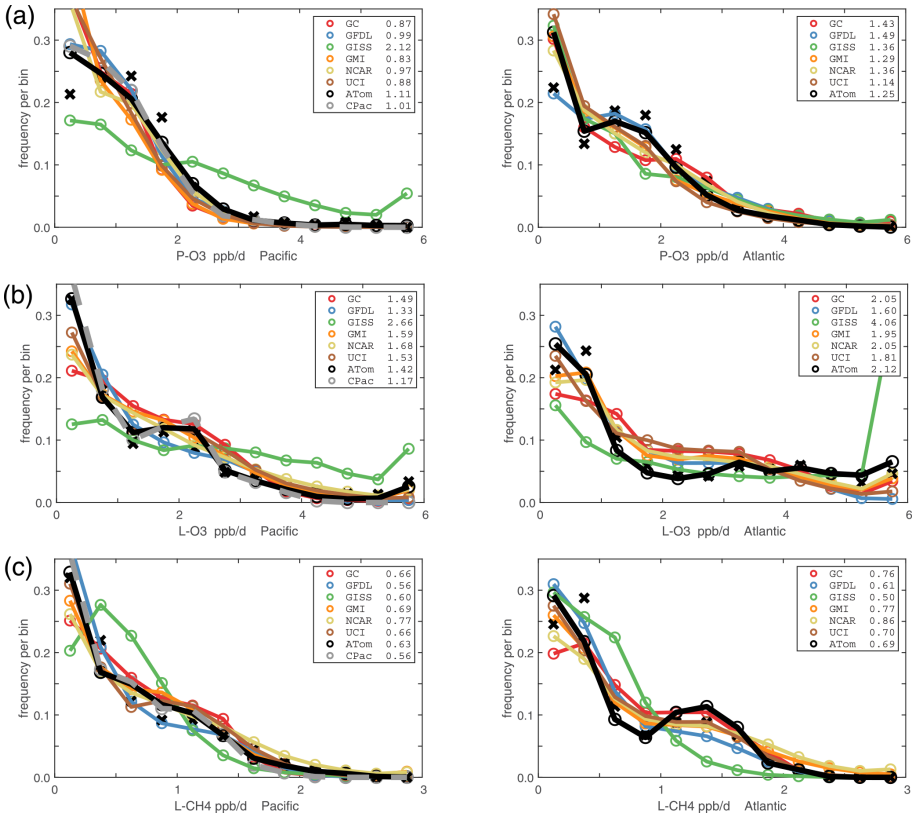

Figure 5. Probability densities (PDs, frequency of occurrence) for the ATom-1 three reactivities (rows: P-O3, L-O3, and L-CH4 in ppb d^{-1}) and for the Pacific and Atlantic from 53° S to 60° N (columns left and right). Each air parcel is weighted as described in the text for equal frequency in large latitude–pressure bins and also by cosine (latitude). The ATom statistics are from the UCIZ model, using MDS-2b and revised RDS* protocol (HNO_4 and PAN damping). The Pacific results (solid black) also show the central Pacific alone (dashed gray). The six models' values for a day in mid-August are averaged over longitude for the domains shown in Fig. S1 and then cosine (latitude)-weighted. Mean values (ppb d^{-1}) are shown in the legend. The PD derived from the ATom 10 s parcels binned into 1° latitude by 200 m altitude (as shown for the tropics in Fig. 2) is typical of a high-resolution global model and denoted by black Xs.

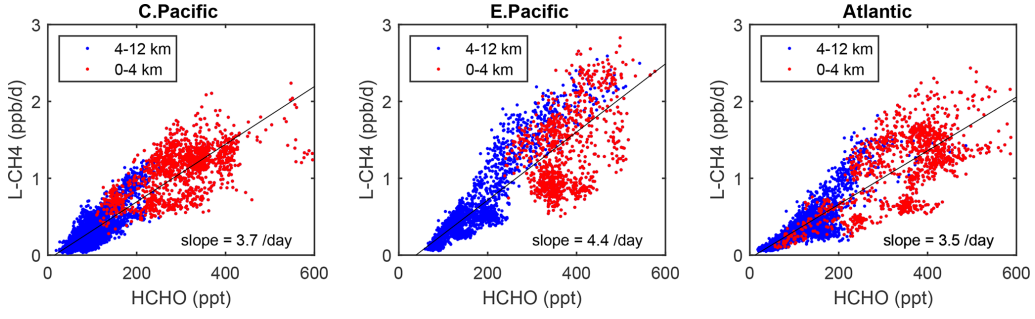

Figure 6. Scatterplot of L-CH4 (ppb d^{-1}) versus HCHO (ppt) for ATom 1 in the three tropical regions shown in Fig. 3. The air parcels are split into the lower troposphere (0–4 km pressure altitude, red dots) where most of the reactivity lies and middle–upper troposphere (4–12 km, blue). A simple linear fit to all data is shown (thin black line), and the slope is given in units of 1 d.

models show a large relative drop in O_3 production below 2 km over the tropical oceans, but ATom shows an increase (C.Pac.), no change (E.Pac.), or a much lesser drop (Atl.). We traced this result to the lack of NO_x at 20–60 ppt levels in the models below 4 km and believe it provides a clear challenge in modeling ozone.

Building our chemical statistics (PDs) from the ATom 10 s air parcels on a scale of 2 km by 80 m, we can identify the fundamental scales of spatial heterogeneity in tropospheric

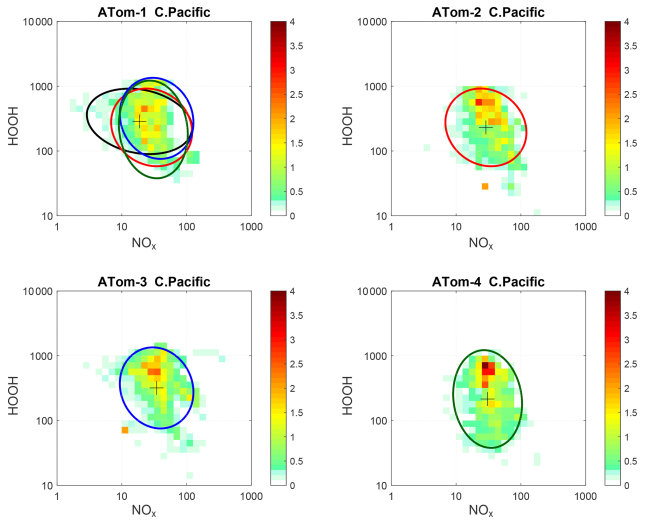

Figure 7. 2D frequency of occurrence (PDs in log ppt mole fraction) of HOOH vs. NO_x for the tropical central Pacific for all four ATom deployments. The cross marks the mean (in log space), and the ellipse is fitted to the rotated PD having the smallest semi-minor axis. The semi-minor and semi-major axes are 2 standard deviations of PD in that direction. The ellipses from ATom-2 (red), ATom-3 (blue), and ATom-4 (dark green) are also plotted in the ATom-1 quadrant.

chemistry. Although heterogeneity occurs at the finest scales (such as seen in some 1 s observations), the majority of variability in terms of the O_3 and CH_4 budgets occurs across scales larger than neighboring 2 km parcels. The PDs measured in ATom can be largely captured by a global model's 100 km by 200 m grid cells in the lower troposphere. This surprising result is evident by comparing the ATom 1D PDs – both species and reactivities – with those from the models' climatologies (Fig. 5). These comparisons show that the modeled PDs are consistent with the innate chemical heterogeneity of the troposphere as measured by the 10 s parcels in ATom. A related conclusion for biomass burning smoke particles is found by Schill et al. (2020), where most of the smoke appears in the background rather than in pollution plumes, and therefore much of the variability occurs on synoptic scales resolved by global models (see their Fig. 1 compared with Fig. 2 here).

5.2 Opportunities and lessons learned

As a quick look at the opportunities provided by the ATom data, we present an example based on the Wolfe et al. (2019) study, which used the F0AM model and semi-analytical arguments to show that troposphere HCHO columns (measurable by satellite and ATom) are related to OH columns (measured by ATom) and thus to CH_4 loss. Figure 6 extends the Wolfe et al. (2019) study using the individual air parcels and plotting L-CH4 (ppb d^{-1}) versus HCHO (ppt) for the three tropical regions where most of the CH_4 loss occurs. The relationship is linear but with a lot of scatter and has slopes ranging from 3.5 to 4.4 per day over the three tropical regions, but for the largest reactivities (0–4 km, 1–3 ppb d^{-1}), L-CH4 is not so well correlated with HCHO.

As is usual with new model intercomparison projects, we have an opportunity to identify model "features" and identify errors. In the UCI model, an error in the lumped alkane formulation (averaging alkanes C_3H_8 and higher) did not show up in P2018, where UCI supplied all the species, but when the ATom data were used, the UCI model became an outlier. Once found, this problem was readily fixed (hence the current UCIZ model version). Inclusion of the F0AM model with its extensive hydrocarbon oxidation mechanism provided an interesting contrast with the simpler chemistry in the global CCM/CTMs. For a better comparison of the chemical mechanisms, we should have F0AM use 5 d of photolysis fields from one of the CTMs. The anomalous GISS results have been examined by a co-author, but no clear causes have been identified as of this publication. The problem goes beyond just the implementation of the RDS protocol, as it shows up in the model climatology (Figs. 4 and 5, also in P2017).

Decadal-scale shifts in the budgets of O_3 and CH_4 are likely to be evident through the statistical patterns of the key species, rather than simply via average profiles. The underlying design of ATom was to collect enough data to develop such a multivariate chemical climatology. As a quick look across the four deployments, we show the joint 2D PDs on a logarithmic scale as in P2017 for HOOH versus NO_x in Fig. 7. The patterns for the tropical central Pacific are quite similar for the four seasons of ATom deployments, and the fitted ellipses are almost identical for ATom 2, 3, and 4. Thus, for these species in the central Pacific, we believe that ATom provides a benchmark of the 2016–2018 chemical state, one that can be revisited with an aircraft mission in a decade to detect changes in not only chemical composition, but also reactivity.

ATom identifies which "highly reactive" spatial or chemical environments could be targeted in future campaigns for process studies or to provide a better link between satellite observations and photochemical reactivity (e.g., eastern Pacific mid-troposphere in August, Fig. 2). The many corollary species measured by ATom (not directly involved in CH_4 and O_3 chemistry) can provide clues to the origin or chemical processing of these environments. We hope to engage a wider modeling community beyond the ATom science team, as in H2018, in the calculation of photochemical processes, budgets, and feedbacks based on all four ATom deployments.

Data availability. The MDS-2b and RDS*-2b data for ATom 1, 2, 3, and 4 are presented here as core ATom deliverables and are posted temporarily on the NASA ESPO ATom website (https://espo.nasa.gov/atom/content/ATom, last access: 1 July 2022; Science team of the NASA Atmospheric Tomography Mission, 2021)

and permanently on Dryad|UCI (https://doi.org/10.7280/D1B12H; Prather, 2022). This publication marks the public release of the reactivity calculations for ATom 2, 3, and 4, but we have not yet analyzed these data, and thus users should be aware and report any anomalous features to the lead authors via haog2@uci.edu and mprather@uci.edu. Details of the ATom mission and data sets are found on the NASA mission website (https://espo.nasa.gov/atom/content/ATom) and in the final archive at Oak Ridge National Laboratory (ORNL; https://daac.ornl.gov/ATOM/guides/ATom_merge.html, last access: 12 December 2022; https://doi.org/10.3334/ORNLDAAC/1581, Wofsy et al., 2018). The MATLAB scripts and data sets used in the analysis here are posted on Dryad (https://doi.org/10.7280/D1Q699; Guo, 2021).

Supplement. The supplement related to this article is available online at: https://doi.org/10.5194/acp-23-99-2023-supplement.

Author contributions. HG, CMF, SCW, and MJP designed the research and performed the data analysis. SAS, SDS, LE, FL, JL, AMF, GC, LTM, and GW contributed original atmospheric chemistry model results. GW, MK, JC, GD, JD, BCD, RC, KM, JP, TBR, CT, TFH, DB, NJB, ECA, RSH, JE, EH, and FM contributed original atmospheric observations. HG, CMF, and MJP wrote the paper.

Competing interests. The contact author has declared that neither they nor their co-authors have any competing interests

Disclaimer. Publisher's note: Copernicus Publications remains neutral with regard to jurisdictional claims in published maps and institutional affiliations.

Acknowledgements. The authors are indebted to the entire ATom Science Team including the managers, pilots and crew, who made this mission possible. Many other scientists not on the author list enabled the measurements and model results used here. The authors thank Xin Zhu for maintaining and updating the UCI chemistry transport model used here. We are grateful for the efforts of the two anonymous reviewers and the editor, Ken Carslaw, for their help in organizing this awkward paper.

Financial support. The Atmospheric Tomography Mission (ATom) was supported by the National Aeronautics and Space Administration's Earth System Science Pathfinder Venture-Class Science Investigations: Earth Venture Suborbital-2. Primary funding of the preparation of this paper at UC Irvine was through NASA (grant nos. NNX15AG57A and 80NSSC21K1454).

Review statement. This paper was edited by Ken Carslaw and reviewed by two anonymous referees.

References

Burkholder, J. B., Sander, S. P., Abbatt, J. P. D., Barker, J. R., Huie, R. E., Kolb, C. E., Kurylo, M. J., Orkin, V. L., Wilmouth, D. M., and Wine, P. H.: Chemical kinetics and photochemical data for use in atmospheric studies: evaluation number 18, Pasadena, CA, Jet Propulsion Laboratory, National Aeronautics and Space Administration, http://hdl.handle.net/2014/45510 (last access: 13 September 2021), 2015.

Charlton-Perez, C. L., Evans, M. J., Marsham, J. H., and Esler, J. G.: The impact of resolution on ship plume simulations with NO_x chemistry, Atmos. Chem. Phys., 9, 7505–7518, https://doi.org/10.5194/acp-9-7505-2009, 2009.

Douglass, A. R., Prather, M. J., Hall, T. M., Strahan, S. E., Rasch, P. J., Sparling, L. C., Coy, L., and Rodriguez, J. M.: Choosing meteorological input for the global modeling initiative assessment of high-speed aircraft, J. Geophys. Res.-Atmos., 104, 27545–27564, https://doi.org/10.1029/1999JD900827, 1999.

Eastham, S. D. and Jacob, D. J.: Limits on the ability of global Eulerian models to resolve intercontinental transport of chemical plumes, Atmos. Chem. Phys., 17, 2543–2553, https://doi.org/10.5194/acp-17-2543-2017, 2017.

Griffiths, P. T., Murray, L. T., Zeng, G., Shin, Y. M., Abraham, N. L., Archibald, A. T., Deushi, M., Emmons, L. K., Galbally, I. E., Hassler, B., Horowitz, L. W., Keeble, J., Liu, J., Moeini, O., Naik, V., O'Connor, F. M., Oshima, N., Tarasick, D., Tilmes, S., Turnock, S. T., Wild, O., Young, P. J., and Zanis, P.: Tropospheric ozone in CMIP6 simulations, Atmos. Chem. Phys., 21, 4187–4218, https://doi.org/10.5194/acp-21-4187-2021, 2021.

Guo, H.: Heterogeneity and chemical reactivity of the remote Troposphere defined by aircraft measurements, Dryad [data set], https://doi.org/10.7280/D1Q699, 2021.

Hall, S. R., Ullmann, K., Prather, M. J., Flynn, C. M., Murray, L. T., Fiore, A. M., Correa, G., Strode, S. A., Steenrod, S. D., Lamarque, J.-F., Guth, J., Josse, B., Flemming, J., Huijnen, V., Abraham, N. L., and Archibald, A. T.: Cloud impacts on photochemistry: building a climatology of photolysis rates from the Atmospheric Tomography mission, Atmos. Chem. Phys., 18, 16809–16828, https://doi.org/10.5194/acp-18-16809-2018, 2018.

Heald, C. L., Coe, H., Jimenez, J. L., Weber, R. J., Bahreini, R., Middlebrook, A. M., Russell, L. M., Jolleys, M., Fu, T.-M., Allan, J. D., Bower, K. N., Capes, G., Crosier, J., Morgan, W. T., Robinson, N. H., Williams, P. I., Cubison, M. J., DeCarlo, P. F., and Dunlea, E. J.: Exploring the vertical profile of atmospheric organic aerosol: comparing 17 aircraft field campaigns with a global model, Atmos. Chem. Phys., 11, 12673–12696, https://doi.org/10.5194/acp-11-12673-2011, 2011.

Myhre, G., Shindell, D., and Pongratz, J.: Anthropogenic and Natural Radiative Forcing, in: Climate Change 2013: The Physical Science Basis, IPCC WGI Contribution to the Fifth Assessment Report, Cambridge University Press, 659–740, https://doi.org/10.1017/CBO9781107415324.018, 2014.

Naik, V., Voulgarakis, A., Fiore, A. M., Horowitz, L. W., Lamarque, J.-F., Lin, M., Prather, M. J., Young, P. J., Bergmann, D., Cameron-Smith, P. J., Cionni, I., Collins, W. J., Dalsøren, S. B., Doherty, R., Eyring, V., Faluvegi, G., Folberth, G. A., Josse, B., Lee, Y. H., MacKenzie, I. A., Nagashima, T., van Noije, T. P. C., Plummer, D. A., Righi, M., Rumbold, S. T., Skeie, R., Shindell, D. T., Stevenson, D. S., Strode, S., Sudo, K., Szopa, S., and Zeng,

G.: Preindustrial to present-day changes in tropospheric hydroxyl radical and methane lifetime from the Atmospheric Chemistry and Climate Model Intercomparison Project (ACCMIP), Atmos. Chem. Phys., 13, 5277–5298, https://doi.org/10.5194/acp-13-5277-2013, 2013.

Prather, M.: NASA Atmospheric Tomography Mission: Modeling and reactivity data sets, Dryad [data set], https://doi.org/10.7280/D1B12H, 2022.

Prather, M. J., Ehhalt, D., Dentener, F., Derwent, R., Dlugokencky, E. J., Holland, E., Isaksen, I., Katima, J., Kirchhoff, V., Matson, P., and Midgley, P.: Chapter 4 – Atmospheric Chemistry and Greenhouse Gases, Climate Change 2001: The Scientific Basis, Third Assessment Report of the Intergovernmental Panel on Climate Change, 239–287, Cambridge University Press, Cambridge UK, ISBN 0521014956, 2001.

Prather, M. J., Zhu, X., Flynn, C. M., Strode, S. A., Rodriguez, J. M., Steenrod, S. D., Liu, J., Lamarque, J.-F., Fiore, A. M., Horowitz, L. W., Mao, J., Murray, L. T., Shindell, D. T., and Wofsy, S. C.: Global atmospheric chemistry – which air matters, Atmos. Chem. Phys., 17, 9081–9102, https://doi.org/10.5194/acp-17-9081-2017, 2017.

Prather, M. J., Flynn, C. M., Zhu, X., Steenrod, S. D., Strode, S. A., Fiore, A. M., Correa, G., Murray, L. T., and Lamarque, J.-F.: How well can global chemistry models calculate the reactivity of short-lived greenhouse gases in the remote troposphere, knowing the chemical composition, Atmos. Meas. Tech., 11, 2653–2668, https://doi.org/10.5194/amt-11-2653-2018, 2018.

Rastigejev, Y., Park, R., Brenner, M. P., and Jacob, D. J.: Resolving intercontinental pollution plumes in global models of atmospheric transport, J. Geophys. Res.-Atmos., 115, D012568, https://doi.org/10.1029/2009JD012568, 2010.

Schill, G. P., Froyd, K. D., Bian, H., Kupc, A., Williamson, C., Brock, C. A., Ray, E., Hornbrook, R. S., Hills, A. J., Apel, E. C., and Chin, M.: Widespread biomass burning smoke throughout the remote troposphere, Nat. Geosci., 13, 422–427, https://doi.org/10.1038/s41561-020-0586-1, 2020.

Science team of the NASA Atmospheric Tomography Mission: ATom, NASA [data set], https://espo.nasa.gov/atom/content/ATom, last access: 13 September 2021.

Stevenson, D. S., Dentener, F. J., Schultz, M. G., Ellingsen, K., Van Noije, T. P. C., Wild, O., Zeng, G., Amann, M., Atherton, C. S., Bell, N., and Bergmann, D. J.: Multimodel ensemble simulations of present-day and near-future tropospheric ozone, J. Geophys. Res.-Atmos., 111, D006338, https://doi.org/10.1029/2005JD006338, 2006.

Stevenson, D. S., Young, P. J., Naik, V., Lamarque, J.-F., Shindell, D. T., Voulgarakis, A., Skeie, R. B., Dalsoren, S. B., Myhre, G., Berntsen, T. K., Folberth, G. A., Rumbold, S. T., Collins, W. J., MacKenzie, I. A., Doherty, R. M., Zeng, G., van Noije, T. P. C., Strunk, A., Bergmann, D., Cameron-Smith, P., Plummer, D. A., Strode, S. A., Horowitz, L., Lee, Y. H., Szopa, S., Sudo, K., Nagashima, T., Josse, B., Cionni, I., Righi, M., Eyring, V., Conley, A., Bowman, K. W., Wild, O., and Archibald, A.: Tropospheric ozone changes, radiative forcing and attribution to emissions in the Atmospheric Chemistry and Climate Model Intercomparison Project (ACCMIP), Atmos. Chem. Phys., 13, 3063–3085, https://doi.org/10.5194/acp-13-3063-2013, 2013.

Stevenson, D. S., Zhao, A., Naik, V., O'Connor, F. M., Tilmes, S., Zeng, G., Murray, L. T., Collins, W. J., Griffiths, P. T., Shim, S., Horowitz, L. W., Sentman, L. T., and Emmons, L.: Trends in global tropospheric hydroxyl radical and methane lifetime since 1850 from AerChemMIP, Atmos. Chem. Phys., 20, 12905–12920, https://doi.org/10.5194/acp-20-12905-2020, 2020.

Stocker, T. F., Qin, D., Plattner, G. K., Tignor, M., Allen, S. K., Boschung, J., Nauels, A., Xia, Y., Bex, V., and Midgley, P. M.: Contribution of working group I to the fifth assessment report of the intergovernmental panel on climate change, Cambridge University Press, 33–115, ISBN 978-1-107-66182-0, 2013.

Tie, X., Brasseur, G., and Ying, Z.: Impact of model resolution on chemical ozone formation in Mexico City: application of the WRF-Chem model, Atmos. Chem. Phys., 10, 8983–8995, https://doi.org/10.5194/acp-10-8983-2010, 2010.

Voulgarakis, A., Naik, V., Lamarque, J.-F., Shindell, D. T., Young, P. J., Prather, M. J., Wild, O., Field, R. D., Bergmann, D., Cameron-Smith, P., Cionni, I., Collins, W. J., Dalsøren, S. B., Doherty, R. M., Eyring, V., Faluvegi, G., Folberth, G. A., Horowitz, L. W., Josse, B., MacKenzie, I. A., Nagashima, T., Plummer, D. A., Righi, M., Rumbold, S. T., Stevenson, D. S., Strode, S. A., Sudo, K., Szopa, S., and Zeng, G.: Analysis of present day and future OH and methane lifetime in the ACCMIP simulations, Atmos. Chem. Phys., 13, 2563–2587, https://doi.org/10.5194/acp-13-2563-2013, 2013.

Wofsy, S. C.: HIAPER Pole-to-Pole Observations (HIPPO): fine-grained, global-scale measurements of climatically important atmospheric gases and aerosols, Philos. T. Roy. Soc. A, 369, 2073–2086, https://doi.org/10.1098/rsta.2010.0313, 2011.

Wofsy, S. C., Afshar, S., Allen, H. M., Apel, E. C., Asher, E. C., Barletta, B., Bent, J., Bian, H., Biggs, B. C., Blake, D. R., Blake, N., Bourgeois, I., Brock, C. A., Brune, W. H., Budney, J. W., Bui, T. P., Butler, A., Campuzano-Jost, P., Chang, C.S., Chin, M., Commane, R., Correa, G., Crounse, J. D., Cullis, P. D., Daube, B.C., Day, D. A., Dean-Day, J. M., Dibb, J. E., DiGangi, J. P., Diskin, G. S., Dollner, M., Elkins, J. W., Erdesz, F., Fiore, A. M., Flynn, C. M., Froyd, K. D., Gesler, D. W., Hall, S. R., Hanisco, T. F., Hannun, R. A., Hills, A. J., Hintsa, E. J., Hoffman, A., Hornbrook, R. S., Huey, L. G., Hughes, S., Jimenez, J. L., Johnson, B. J., Katich, J. M., Keeling, R. F., Kim, M. J., Kupc, A., Lait, L. R., Lamarque, J.-F., Liu, J., McKain, K., Mclaughlin, R. J., Meinardi, S., Miller, D. O., Montzka, S. A, Moore, F. L., Morgan, E. J., Murphy, D. M., Murray, L. T., Nault, B. A., Neuman, J. A., Newman, P. A., Nicely, J. M., Pan, X., Paplawsky, W., Peischl, J., Prather, M. J., Price, D. J., Ray, E. A., Reeves, J. M., Richardson, M., Rollins, A. W., Rosenlof, K. H., Ryerson, T. B., Scheuer, E., Schill, G. P., Schroder, J. C., Schwarz, J. P., St.Clair, J. M., Steenrod, S. D., Stephens, B. B., Strode, S. A., Sweeney, C., Tanner, D., Teng, A. P., Thames, A. B., Thompson, C. R., Ullmann, K., Veres, P. R., Vieznor, N., Wagner, N. L., Watt, A., Weber, R., Weinzierl, B., Wennberg, P. O., Williamson, C. J., Wilson, J. C., Wolfe, G. M., Woods, C. T., and Zeng L. H.: ATom: Merged Atmospheric Chemistry, Trace Gases, and Aerosols, ORNL DAAC [data set], Oak Ridge, Tennessee, USA, https://doi.org/10.3334/ORNLDAAC/1581, https://daac.ornl.gov/ATOM/guides/ATom_merge.html (last access: 12 December 2022), 2018.

Wolfe, G. M., Nicely, J. M., Clair, J. M. S., Hanisco, T. F., Liao, J., Oman, L. D., Brune, W. B., Miller, D., Thames, A., Abad, G. G., and Ryerson, T. B.: Mapping hydroxyl variability throughout the global remote troposphere via synthesis of airborne and satel-

lite formaldehyde observations, P. Natl. Acad. Sci. USA, 116, 11171–11180, https://doi.org/10.1073/pnas.1821661116, 2019.

Young, P. J., Archibald, A. T., Bowman, K. W., Lamarque, J.-F., Naik, V., Stevenson, D. S., Tilmes, S., Voulgarakis, A., Wild, O., Bergmann, D., Cameron-Smith, P., Cionni, I., Collins, W. J., Dalsøren, S. B., Doherty, R. M., Eyring, V., Faluvegi, G., Horowitz, L. W., Josse, B., Lee, Y. H., MacKenzie, I. A., Nagashima, T., Plummer, D. A., Righi, M., Rumbold, S. T., Skeie, R. B., Shindell, D. T., Strode, S. A., Sudo, K., Szopa, S., and Zeng, G.: Preindustrial to end 21st century projections of tropospheric ozone from the Atmospheric Chemistry and Climate Model Intercomparison Project (ACCMIP), Atmos. Chem. Phys., 13, 2063–2090, https://doi.org/10.5194/acp-13-2063-2013, 2013.

Young, P. J., Naik, V., Fiore, A. M., Gaudel, A., Guo, J., Lin, M. Y., Neu, J. L., Parrish, D. D., Rieder, H. E., Schnell, J. L., and Tilmes, S.: Tropospheric Ozone Assessment Report: Assessment of global-scale model performance for global and regional ozone distributions, variability, and trends, Elementa, 6, 10, https://doi.org/10.1525/elementa.265, 2018.

Yu, K., Jacob, D. J., Fisher, J. A., Kim, P. S., Marais, E. A., Miller, C. C., Travis, K. R., Zhu, L., Yantosca, R. M., Sulprizio, M. P., Cohen, R. C., Dibb, J. E., Fried, A., Mikoviny, T., Ryerson, T. B., Wennberg, P. O., and Wisthaler, A.: Sensitivity to grid resolution in the ability of a chemical transport model to simulate observed oxidant chemistry under high-isoprene conditions, Atmos. Chem. Phys., 16, 4369–4378, https://doi.org/10.5194/acp-16-4369-2016, 2016.

Zhuang, J., Jacob, D. J., and Eastham, S. D.: The importance of vertical resolution in the free troposphere for modeling intercontinental plumes, Atmos. Chem. Phys., 18, 6039–6055, https://doi.org/10.5194/acp-18-6039-2018, 2018.

Supplement of Atmos. Chem. Phys., 23, 99–117, 2023
https://doi.org/10.5194/acp-23-99-2023-supplement

Atmospheric Chemistry and Physics Open Access

Supplement of

Heterogeneity and chemical reactivity of the remote troposphere defined by aircraft measurements – corrected

Hao Guo et al.

Correspondence to: Hao Guo (haog2@uci.edu) and Michael J. Prather (mprather@uci.edu)

S.1. The ATom Modeling Data Stream version 2b (MDS-2b)

The ATom mission was designed to collect a multi-species, detailed chemical climatology that documents the patterns of physical and chemical heterogeneity throughout the remote troposphere. The calculation of reactivities requires a complete set of key species in each air parcel to initialize chemistry models and then calculate the CH_4 and O_3 reactivities over a 24 h cycle. The ATom Modeling Data Stream (MDS) provides a semi-continuous set of 10 s air parcels with a full set of values for the key chemical reactants and conditions. This Supplementary Methods Section documents the methods used to create the MDS versions.

The original MDS version 0 used CO or other surrogates and correlations with CO to fill gaps. MDS-0 was distributed to 6 modeling groups who then calculated the mean reactivities and photolysis rates using the ATom protocol for 3D models (initialize a model grid cell nearest the observation with the ATom key species from the MDS, integrate for 24 h without transport or other physical connection between cells, average the reactivities over 5 days scattered 5-days apart throughout the mission). Reported reactivities are the 5-day averages. These first results are reported here because they allow for a cross-model comparison using the same MDS for initialization. After examining the statistics of the gap-filled parcels, we found that many MDS-0 species were poorly interpolated and the abundances of VOCs and NOx were sometimes exaggerated. We tried to correct these errors with MDS-1 and tested this version with the UCI and GMI models. Again, we found that the gap filling failed. Then we started on the formal and careful protocol MDS version 2 described here, which is transparent (flags describe how each datum point is determined). We calculated these reactivities with the UCI CTM only. Our first look at the reactivities showed that the Eastern Pacific was unusually reactive in ATom-1. We found that the MDS-2 method of long-gap filling for NOx resulted in propagation of high NOx levels from the over-land profiles into the over-water profiles in the tropics. We separated these two set of profiles used for long-gap NOx filling and created an updated version MDS-2b. This is the final version at the time of this paper.

ATom completed its four deployments: ATom-1 starting 20160729 (YYYMMDD), ATom-2 starting 20170126, ATom-3 starting 20170928, and ATom-4 starting 20180424. ATom targets the remote troposphere by sampling over the middle of the Pacific and Atlantic Ocean basins. The DC-8 aircraft performed in situ profiling of the atmosphere from 0.2 km to 12 km along each flight segment as often as possible. Each deployment lasted about 4 weeks and contained 11 to 13 research flights (RF). Fig. S1 maps the 48 RF, and the Table S1 summarizes each flight in terms of airports, starting date (UT), and number of 10 s parcels. We also number all the research flights consecutively as ATom flights (AF) 1 through 48. The 10 s data starts with 149,133 parcels, but we collapse this to 146,494 parcels, avoiding near-airport pollution, to make MDS version 2b (MDS-2b) described here. AF 46 is a short ferry flight from Kangerlussuaq, Greenland to Bangor, Maine with many instruments turned off and no profiling, thus these 1,106 parcels contain only flight data (MDS variables 1:11) and no chemical data.

ATom sampling of the troposphere is more uniform than most aircraft missions, but still contains some biases that can be adjusted by weighting each air parcel. Due to the typical profiling sequence (level at cruising attitude for 10 min, descent for 20 min, level flight about 160 m above the sea level for 5 min, and a 20-min climb back to cruising altitude) and to the occasional requirements of weather or air traffic control, the sampling is skewed towards the uppermost troposphere ($P < 300$ hPa) and, secondly, the marine boundary layer. For certain analyses such as probability densities (PDs) we recommend weighting each parcel inversely with the density of sampling (e.g., the number of parcels in a 10° latitude by 100 hPa pressure bin). These bins are used only for weighting each parcel and do not average the values. No parcel weights are

included in MDS-2. The ATom-1 analysis selects three study domains: Global includes all parcels (32,383) weighted as above; Pacific considers all measurements over the Pacific Ocean from 53 °S to 60 °N (research flights RF 1,3,4,5,6); and the Atlantic, likewise, from 53 °S to 60 °N (RF 7, 8, 9) over the Atlantic basin. The ATom-1 flight tracks shown in Fig. S1 identify the Pacific and Atlantic domains with very thick lines. Also shown are the regional blocks used to calculate the model climatologies for one day in mid-August over those domains.

We choose 10 s averages for our air parcels as a compromise to include most of the instruments, and because the 10 s merged data is a standard product (Wofsy et al., 2018). Some of our core species are measured with gas chromatographs or flask samples with longer integrations times (30-90 sec), but these can be mapped onto the 10 s parcels with loss of the higher frequency variability found in the 10 s measurements. The frequent profiling of the DC-8 gives us both vertical and horizontal scales: the vertical extent of a 10 s parcel is 50–110 m (55 %–95 % of all parcels, with < 50% having near level flight) and the horizontal extent is typically 1.4–2.5 km (10 %–90 % of all parcels). A few key species have 1 Hz measurements, and, as a case study, we examine the time series of O_3 and H_2O measured during one of the profiles of ATom-1 RF 3 in Fig. S2. The 1 s data is plotted along with the 10 s averages. Most of the heterogeneity including correlated variability is caught with the 10 s parcels. For all of RF 3, the root mean square error (RMSE) of the 10 s averages linearly interpolated to 1 s is 6 % for H_2O and 3 % for O_3. The short-gap interpolation described below has an RMSE twice as large for these same species. A typical global model resolution is indicated in Fig. S2 by the vertical lines spaced at 500 m altitude intervals.

The challenge in creating the MDS is the merging of multiple measurements of the same species and filling gaps in the record. MDS includes the core reactive species (H_2O, O_3, CO, CH_4, NOx, NOxPSS, HNO_3, HNO_4, PAN, CH_2O, H_2O_2, CH_3OOH, acetone, acetaldehyde, C_2H_6, C_3H_8, *i*-C_4H_{10}, *n*-C_4H_{10}, alkanes, C_2H_4, alkenes, C_2H_2, C_5H_8, benzene, toluene, xylene, CH_3ONO_2, $C_2H_5ONO_2$, $RONO_2$, CH_3OH) and corollary species indicative of pollution or processing (HCN, CH_3CN, SF_6, relative humidity, aerosol surface area (4 modes), and cloud indicator), see Table S2. Every species in each air parcel is now flagged so that the instrument is clearly identified (in the case that two instruments measure the same species) and the type of the gap filling (dependent on the length of the gap) is denoted so that the users can develop their own criteria for including, or not including, the gap-filled species. Flags 1 & 2 indicate a reported measurement from a primary (1) or secondary (2) instrument. Flag 3 means short-gap filling. Flags 4 & 6 indicate log-gap filling for tropospheric and stratospheric parcels, respectively. Flag 5 applies to missing flights with no data from that instrument(s), and these were filled by a multiple linear regression from the parallel flights. Flag 0 indicates not a number (NaN), which only occurs for AF 46. Thus, while the MDS creates a continuous stream of fully speciated 10 s air parcels, the users can sub-select, for example, only the direct measurements from the primary instrument.

S.1.1. The primary ATom data sets

The 'Mor' data sets created by Wofsy et al. (2018) contain merges of the ATom 10 s data (Mor.all), the WAS flask data analyzed post-flight (Mor.WAS.all) and the in-flight TOGA chromatograph-mass spectrometer data (Mor.TOGA.all). These data sets are released in a gzip file with the YYYY-MM-DD of their creation. For this MDS version (2020-05-27), we use the following 3 data sets:

'Mor.all.at1234.2020-05-27.tbl' (653,494,900 bytes)
'Mor.WAS.all.at1234.2020-05-27.tbl' (49,091,169 bytes)
'Mor.TOGA.all.at1234.2020-05-27.tbl' (80,579,206 bytes)

The Mor data are ASCII text files with extremely long records and difficult to read, containing a mix of comma-separated floating point, integer and character strings. For Mor.all, the 149133 records contain 675 comma-separated variables (but this can change with different releases). Some of the floating point variables are longer than 20 characters due to excess precision in the scientific notation. We pre-process these with a Fortran generic read(5,*) using the comma separation to generate character strings. The code searches the title (first) record of the Mor…tbl to identify the specific columns that we need for MDS (in this case 39 out of 675). The 39 key data from each record are rewritten in formatted form (39a40, because some floating point variables were excessively long and 39a20 was inadequate) with comma separation. All numerical values are copied verbatim, but the text 'NA' is replaced by 'NaN'. This new file can be simply imported into Matlab or more easily read by other software. Further, this approach ensures that the correct quantities are pulled from the Mor…tbl file, even if the column order changes due to addition or removal of data. The WAS and TOGA observations have separate files with the start and end times of the observed air mass, which is greater than the 10s interval in the regular file. Both WAS & TOGA Mor…data sets have a large number of data columns (729 & 727) with fewer records (6,991 & 12,168, respectively).

The 3 Fortran output files are imported into Matlab (using 'Import Data') and then processed as described below. The instructions and Matlab code are included in text files containing Matlab commands: 'Pmat-Mor1.txt', 'Pmat-WAS+TOGA.txt', 'Pmat-MDS0n.txt').

S.1.2. Preliminary processing and identifying gaps

In terms of critical flight data (time, latitude, longitude, altitude), there are no gaps in the record. UTC_stop has a gap, but this variable is not used in the MDS (10s intervals are assumed).

The Mor.all.at1234.2020-05-27 data set of 149,133 10s parcels was sorted into deployments and research flights. The beginning and end points of each research flight (RF) along with the deployment and starting date of each flight are given in Table S1. All together there are 48 flights, but AF 46 contains only flight data. All three types of Mor data include some measurements close to the airports, which often have ground-level pollution. We remove these data by including only measurements at altitudes of 900 m or more above the takeoff/landing airport. The record collapses to 146,494 parcels, also shown in Table S1.

The list of MDS-2b variables, their MDS identifiers (all ending in _M) and the sources in standard ATom nomenclature are given in Table S2. The flag variables (0 to 6) are also explained there. Information about each research flight is summarized in **Table S3abcd**, including the average latitude, longitude and altitude of the 10s parcels (all equally weighted here). The abcd sub-tables correspond to the 4 deployments. For each of the MDS variables 12 to 50, The % of non-NaN values with flags = 1, 2 or 3, is shown (the remaining % has flags = 4, 5 or 6). These data correspond to a primary or secondary direct measurement (1 or 2) or else short-gap interpolation (3, see text below). Missing data for an entire flight (0%) has shaded cells.

Mor.all combined species and fixes. The primary MDS NOx values were created by simply summing NO_CL + NO2_CL before any attempt to deal with the negative values. The number (27071) of NOx NaNs coincides with those of NO2_CL. The alternative photostationary state NOx values (NOxPSS) were calculated from O_3, NO and J-values and was originally proposed as a more accurate value for NOx. Subsequent analysis has shown this approach is biased, and it is included here only for ATom-1 because some early model studies used it in the MDS-0 version. A small number (22) of CH4_QCLS values have unrealistic abundances <1000 ppb and these are converted to NaNs. The NaNs in these cases were filled using the algorithm below.

TOGA and WAS combined species and immediate fixes. Methyl and ethyl nitrate (WAS only) are kept separately but the 6 higher organo-nitrates are combined into $RONO_2$; the limited TOGA organo-nitrates are not used. For both WAS and TOGA, toluene and ethylbenzene are combined into toluene, and the two forms of xylene are combined. Both forms of butane are kept, but higher alkanes are combined into 'Alkanes' for both TOGA and WAS. TOGA and WAS use -888 flags for LLOD and these are converted to 0.001 ppt because the LLOD values for these species (e.g., 3 ppt) are much higher than remote background values and setting them to the LLOD level would be misleading. TOGA's toluene has some mistaken values of 888 and 999 instead of -888 and -999 and these are corrected. All -999 values, as well as all gaps in either TOGA or WAS measurement intervals are converted to NaNs. The WAS and TOGA data have time stamps (stop minus start) much longer than the 10 s parcels in the Mor.all data sets, and their values are mapped onto the 164,494 parcels whenever their start or stop time falls within the 10s start-stop range, else they are filled with NaNs. The WAS and TOGA instruments sample air averaged over typically 30 to 90 s, and then have a gap before the next measurement, varying from 30 to 300 s. The TOGA length-of-measurement is regular with the 10–90 percentile range being about 35 s and the same percentile length-of-gaps being about 85 s. The WAS data comes from flasks filled in flight, and the time to fill a flask depends on the pressure, and the gap depends on the operator decision: the 10%-90%ile length-of-measurement is 32 to 90 s, and the corresponding gaps are 33 to 285 s.

S.1.3. Interpolation and fill of data gaps

The actions here are arbitrary but judicious, and every attempt was made to avoid introducing spurious data. There are a number of negative values for chemical variables that are intrinsically positive definite. Instrument reporting of a negative value is expected when the concentration is near the limit of detection or within the instrumental noise range. The MDS choice is simply to take all such values less than or equal to 0 and convert to 0.001 ppt. Since these negative values usually represent a small concentration close to the detection limit, they have little impact on the chemistry calculations using the MDS. If analyzing statistics near this range, the original Mor data sets should be used.

Pressure and temperature. P and T have 5 very small gaps of length ~6 (# of 10s parcels missing) plus a longer gap of length 28. All gaps occurred during smooth descent or ascent and so were filled using linear interpolation. These are denoted by flag_M(:,10) = flag_M(:,11) = 3. In this document we are careful to give measured species a suffix that denotes their provenance, and thus the MDS variables denoting the combined, continuous data are labeled P_M and T_M.

H_2O and relative humidity. There are a number of short gaps in the record of H_2O_DLH and RHw_DLH, and only 2 longer gaps (length = 83 and 87). One of the long gaps occurs during descent as H_2O jumps from 240 to 18,000 ppm. Thus we choose a linear in the log method for all H_2O gaps, while a simply linear method is used to fill RHw gaps. These are denoted by flag_M(:,12) = flag_M(:,13) = 3. The MDS variables denoting the combined data are H2O_M and RHw_M.

CO. In our first attempts to produce a gap-filled record for chemical modeling, we sought a species with continuous measurement that could be used as a proxy for unusual or polluted air during the gaps in other species. CO was the obvious species because it is indicative of biomass burning or industrial pollution, and ATom has two well calibrated, nearly continuous measurements: CO_NOAA and CO_QCLS. The primary CO data are from QCLS because it has higher precision and the secondary are from NOAA which has fewer gaps. Unfortunately, after

creating this gap-filled CO data and applying it as a proxy for MDS versions 0 and 1, we found that CO had little skill in filling the gaps in other species. We use this method to generate our CO_M record for the MDS, but do not use it for other species. This processing of the CO data was done with the full 149,133-parcel dataset, and not the airport-collapsed data set. For the MDS-2b airport-truncated data set, CO_NOAA has 8463 gaps; and CO_QCLS has 30,233. Most all of these gaps are short and part of the instrument cycling.

1. Modify CO_QCLS: interpolate short gaps in the CO_QCLS record (≤10 parcels = 100s ~ 1000 m vertically)
2. Create a continuous CO_N record.
    a. Start with CO_NOAA and locate all the NaN gaps.
    b. Fill gaps with modified CO_QCLS where available and locate new NaN gaps.
    c. Average CO for 5 points on either side of gap, interpolate linearly across the gaps.
3. Smooth the CO_N record, which is visibly noisy at 10 s with 11-point running average (~ 1000 m in vertical).
4. Create a continuous CO record.
    a. Define CO = modified CO_QCLS (step 1).
    b. Fill the gaps in CO with CO_N (step 3).
    c. Define CO flags:
        1 = primary, QCLS (116,261 parcels);
        2 = secondary, smoothed CO_N (29428);
        3 = modified, short-interpolated QCLS (80);
        4 = interpolated CO_N (725).

Two samples of this CO interpolation method are shown in Fig. S3. The frequency of occurrence of all flags for this new CO_M variable, along with the other MDS chemical variables, are given in Table S4. About 99 % of the CO_M records are from direct measurements (QCLS or NOAA), and this is matched only by the H_2O and O_3 measurements.

Short-gap simple interpolation for remaining species. It was decided that the least intrusive method for filling short data gaps was to simply interpolate using only the instrument data. In MDS versions 0 and 1, CO was used as a proxy to fill these gaps, but later analysis showed little correlation with absolute CO or even the short-term variability in CO. We examined the typical size of gaps and their frequency. For the Mor.all species we selected gaps of ≤ 13 for short-gap interpolation; for WAS the gap frequency peaked about 10 (100 s) and we selected gaps of ≤10; for TOGA there was a strong peak at gap length of 7-8 (instrument cycle time) and we also selected ≤ 10 as the criterion. These gaps correspond to about 1000 m or less in the vertical during ascent or descent. For most Mor.all variables this adds about 10 % (absolute) to the number of non-NaN parcels, but for WAS and TOGA with many smaller gaps it greatly enhances the coverage. WAS coverage goes from 28 % to 41 %, while TOGA jumps from 31% to 93% because most gaps are 85 s. For all short-gap interpolation, the parcel data for that species is tagged with flag = 3.

Long-gap interpolation for remaining species - Troposphere. We choose a robust and minimally intrusive method for filling gaps > 10 (100 s) based upon the average tropospheric profile for that flight, using eight 100-hPa-wide bins (< 300, 300–400, 400–500, 500–600, 600–700, 700–800, 800–900, > 900 hPa). The gap value is replaced by the appropriate bin value. If any bins have no measured values, we use the nearest bin or average of the nearest bins. It is important not to confuse stratospheric and tropospheric air when gap filling. From our analysis, a number of key reactive species (e.g., CH_2O, HOOH, NOx) show distinctly different patterns as ATom crosses into the stratosphere. This method had to be refined in version 2b, particularly for the first research flight of each deployment (Palmdale to the Equator and back along 121 ºW).

We found high NOx values on the climb out of or into the Los Angeles basin were mapped onto the tropical ocean where the instrument dropped out for many profiles, especially in ATom-1. We created two separate average NOx profiles as described above: one for east of 121 ºW and another for over the ocean. This special fix was only applied to NOx to create version 2b.

Long-gap interpolation - Stratosphere. We find the most robust definition of stratospheric-like air to be based primarily on H_2O rather than O_3, because O_3 abundances > 200 ppb are often seen in large, clearly tropospheric air masses with H_2O > 50 ppm. Based on percentiles of O_3 at different values of H_2O (see Fig. S4a) we pick <30 ppm as the criteria for being stratospheric, with the secondary requirements that O_3 > 80 ppb and CO < 120 ppb (see Fig. S4b). For the stratospheric air we create mean 'profiles' in terms of six O_3 bins (< 200, 200–300, 300–400, 400–500, 500–700, > 700 ppb) use this as a lookup table for gap filling. There are many fewer stratospheric parcels, and the stratosphere tends to be similar across latitudes, and so we create a single lookup tables from all research flights at all latitudes. In general, these near tropopause air parcels are cold and dry and not highly reactive; however when partitioning the chemistry model calculated reactivities between stratosphere and troposphere, these criteria may need to be re-investigated.

As a measure of the error in this long-gap interpolation, we randomly select 10% of the air parcels from data stream before calculating the long-gap interpolation, interpolate those 10% points, and calculate the mean bias and root-mean-square error (rmse). This is repeated 10 times and we show the average results in Table S5 below. We find these results acceptable, and better than the multiple linear regressions we tried. There may be a better way to do this in future versions MDS-2b, perhaps with a machine-learning approach. Gaps interpolated in this way are given flag = 4 (troposphere tables) and flag = 6 (stratosphere tables).

Missing data for an entire flight. For **ATom-1 RF-5**, an instrument failed and we lost all data for H2O2_M, HNO3_M, and HNO4_M. This flight was from American Samoa to Christ Church. We fill these species using a multiple linear regression from the parallel flights ATom-1 RF-4 and ATom-2/3/4 RF-4/5. The independent (explanatory) variables for the multiple linear regression for these missing flights are chosen to be pressure, noontime solar zenith angle and latitude (in that order). For H2O2_M and HNO3_M, we calculate the missing ATom-1 RF-5 data using the full set of parallel flights, but for HNO4_M, we can use only ATom-1/2 flights (see Table S3 & S6). Data filled for missing flights are given flag = 5. For **ATom-2 RF-2**, we also lost all data for H2O2_M, HNO3_M, and HNO4_M. In this case the regression is based on parallel flights ATom-2 RF-3 and ATom-1/3/4 RF-2/3 for H2O2_M and HNO3_M, but only ATom-2 RF-3 and ATom-1 RF-2/3 for HNO4_M. For **ATom-3 RF-1**, we lost all data for NOx_M. A multiple linear regression is based on parallel flights ATom-3 RF-2 and ATom-1/2/4 RF-1/2. For **ATom-3/4 all,** we lost all data for HNO4_M, and the best we can do is base the regression on all HNO4_M measurements (not filled as noted above) from ATom-1/2. This is clearly one of the weakest gap filled here, and users should be careful if key results depend HNO4_M values for ATom-3/4. For **ATom-4 RF-5/6/7/8/9/12/13**, we lost all data for CH3OOH_M. A multiple linear regression approach was based on data from the preceding RF-4 as well as the parallel research flights from the other 3 deployments (i.e., ATom-1/2 RF-5 to 11, ATom-3 RF-5 to 13, ATom-4 RF-4). For **ATom-4 RF-11** (AF 46), all chemical data have flag = 0, value = NaN. A summary of the missing flights and species along with estimated error in our gap filling is given in Table S6.

From the reactivity results for ATom-1 shown in this paper, the lack of ATom-3 NOx observations in the Eastern Pacific (RF 1) mean that the P-O3 statistics there (not calculated in this paper) will not be useful.

S.1.4. Species measured by two instruments

Several species have redundant measurements and these are identified by the duplicate sources in Table S2. The choice of primary (flag = 1) and secondary (flag = 2) are chosen based on continuity of record or coverage of related species, or our estimate of the higher precision measurement. Primary data sources usually have a better data coverage.

CH_4: (1) CH4_NOAA, (2) CH4_QCLS. The primary has more data and does not have spurious anomalies. There is no evident bias, but some scatter, and so the NaNs in the primary record (which first has had short-gap interpolation as noted above) are simply filled with the secondary record (also with short-gap interpolation).

CH_2O: (1) CH2O_ISAF, (2) CH2O_TOGA. Formaldehyde is a key reactive species and TOGA provides a secondary record for the 2nd half of ATom-4 when ISAF failed. The overlapping data with both instruments is plotted in below (Fig. S5). The mean difference in overlapping observations is very small (-1 out of a mean of 134 ppt), but the rms is larger (75 ppt). ISAF has a number of values > 1000 ppt, while TOGA has none. A linear fit gives a slope of 0.8 with R^2 = 0.59, but a 1:1 slope has only slightly smaller R^2 = 0.55. We do not attempt to rescale the TOGA data in this case and just replace any NaNs remaining in the short-gap-interpolated ISAF record (particularly flights 42:48) with TOGA data (also short-gap interpolated).

PAN: (1) PAN_GTCIMS, (2) PAN_PECD*. The GTCIMS joined the mission at ATom-2. The overlap period shows a clear bias between the GTCIMS and PECD observations. A linear fit is clear (R^2 = 0.84), and we rescale the secondary PECD* = (PECD + 0.45)/1.18.

C_3H_8: (1) Propane_WAS, (2) Propane_TOGA. No obvious bias is found. A linear fit gives an R^2 = 0.90, but the 1:1 line has an R^2 = 0.85, so we just use the TOGA data directly as the secondary observation.

***i*-C_4H_{10}: (**1) iButane_WAS, (2) iButane_TOGA. No obvious bias is found. A linear fit gives an R^2 = 0.955, but the 1:1 line has an R^2 = 0.947, so we just use the TOGA data directly as the secondary observation.

***n*-C_4H_{10}: (**1) nButane_WAS, (2) nButane_TOGA. No obvious bias is found. A linear fit gives an R^2 = 0.962, but the 1:1 line has an R^2 = 0.942, so we just use the TOGA data directly as the secondary observation.

C_5H_8: (1) Isoprene_TOGA, (2) Isoprene_WAS. No obvious bias is found. A linear fit gives an R^2 = 0.938, but the 1:1 line has an R^2 = 0.904, so we just use the WAS data directly as the secondary observation.

benzene: (1) Benzene_TOGA, (2) Benzene_WAS. The is some systematic difference between WAS and TOGA (TOGA = ~0.75 x WAS), but the contribution of WAS to the aromatics is small (see flag=2 is <3% in **Table S4**) and so we did not scale WAS.

toluene: (1) Toluene_TOGA + EthBenzene_TOGA, (2) Toluene_WAS + EthBenzene_WAS. No obvious bias is found in spite of the large scatter. A linear fit gives an R^2 = 0.75, but the 1:1 line has an R^2 = 0.74, so we just use the TOGA data directly as the secondary observation.

xylene: (1) mpXylene_TOGA + oXylene_TOGA, (2) mpXylene_WAS + oXylene_WAS. No obvious bias is found in spite of the very large scatter. A linear fit gives an $R^2 = 0.3$, so we just use the WAS data directly as the secondary observation.

HCN: (1) HCN_CIT, (2) HCN_TOGA. The CIT observation is chosen as primary because of its more continuous, 10s record. In spite of the large scatter, a linear fit with a slope of 0.8 does not greatly reduce the variance ($R^2 = 0.74$ vs 0.65 for 1:1), so we just use the TOGA data directly as the secondary observation.

SF6: (1) SF6_PECD, (2) SF6_UCATS. The scatter seems large, but the relationship is mostly 1:1 with $R^2 = 0.90$. A linear fit gives a slope of 0.99, and so we just use the UCATS data directly as the secondary observation. Both data sets are sparse.

S.2. The Reactivity Data Stream

In this paper, we use 6 global atmospheric chemistry models for their August chemical statistics. We use 5 of these models plus a box model to calculate the Reactivity Data Stream (RDS, i.e., chemical tendencies) for each ATom-1 MDS-0 10 s air parcel. The models are summarized in the main paper Table 1 and with more detail in Table S7 here. Statistics of the reactivities and J-values across models and MDS versions are shown in the main Table 2 and Tables S8abc here. Table S9 gives the standard deviation when averaging across 5 separated days in August (% of mean reactivity or J-value). See the main paper for a description of the RDS protocol used for MDS-0 and the updated RDS* protocol used for MDS-2b.

426

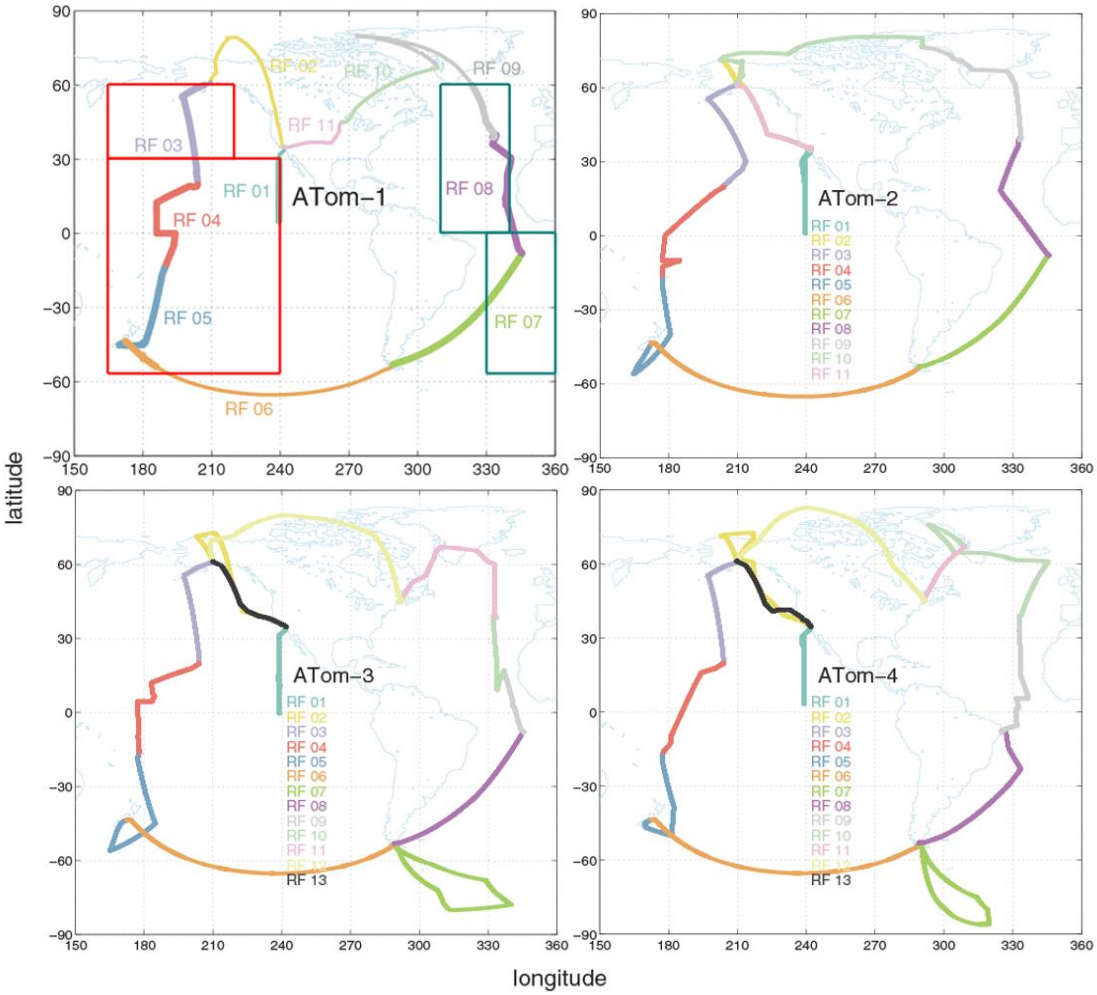

Fig. S1. Flight tracks for the 4 ATom deployments. For ATom-1, the flight segments considered Pacific and Atlantic domains for this paper are shown with very thick lines. The corresponding blocks used for model climatologies are outlined with rectangles: Pacific, red; Atlantic, blue-green.

427

428

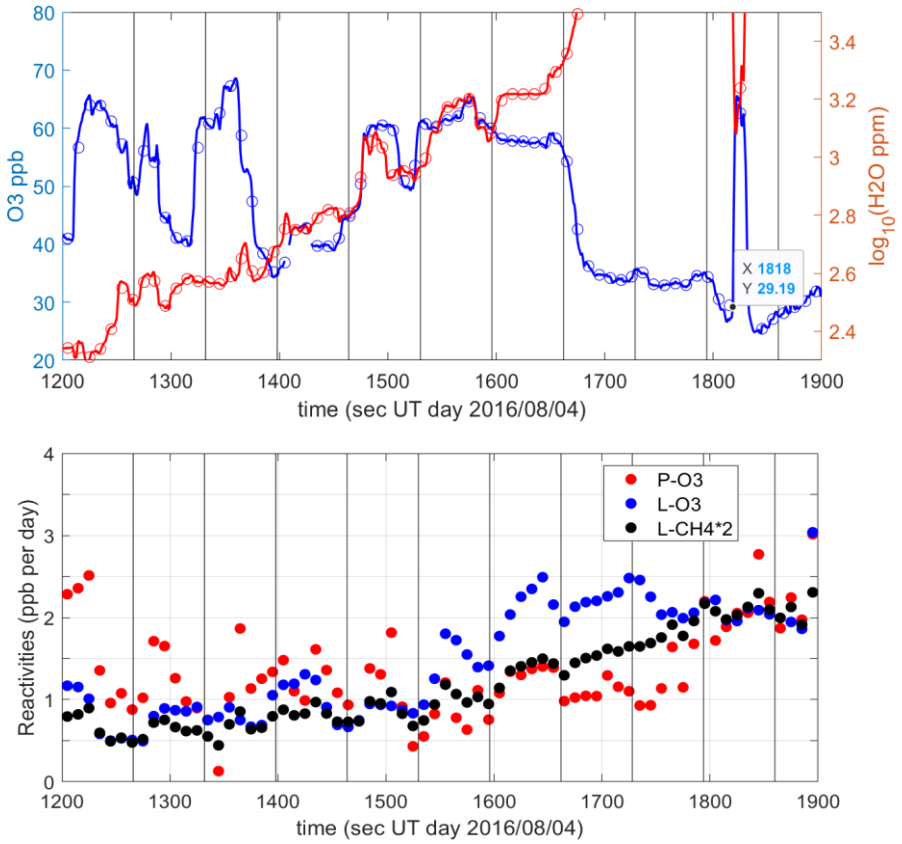

Fig. S2. Profile during a descent on the Anchorage-Kona flight (ATom-1, RF-3, 31° N). The profile here begins at 7.2 km (1200 s) and ends at 2.1 km (1900 s, H_2O is cut off). (a) Fine structure in O_3 (ppb) and H_2O (log_{10}, ppm) at 1 s (solid line) and 10 s (open circles) resolution. (b) Reactivities for the 10 s parcels calculated with the UCI CTM. Descent rate averaged 7.5 m/s, and vertical lines indicate 500 m thick layers.

429

430

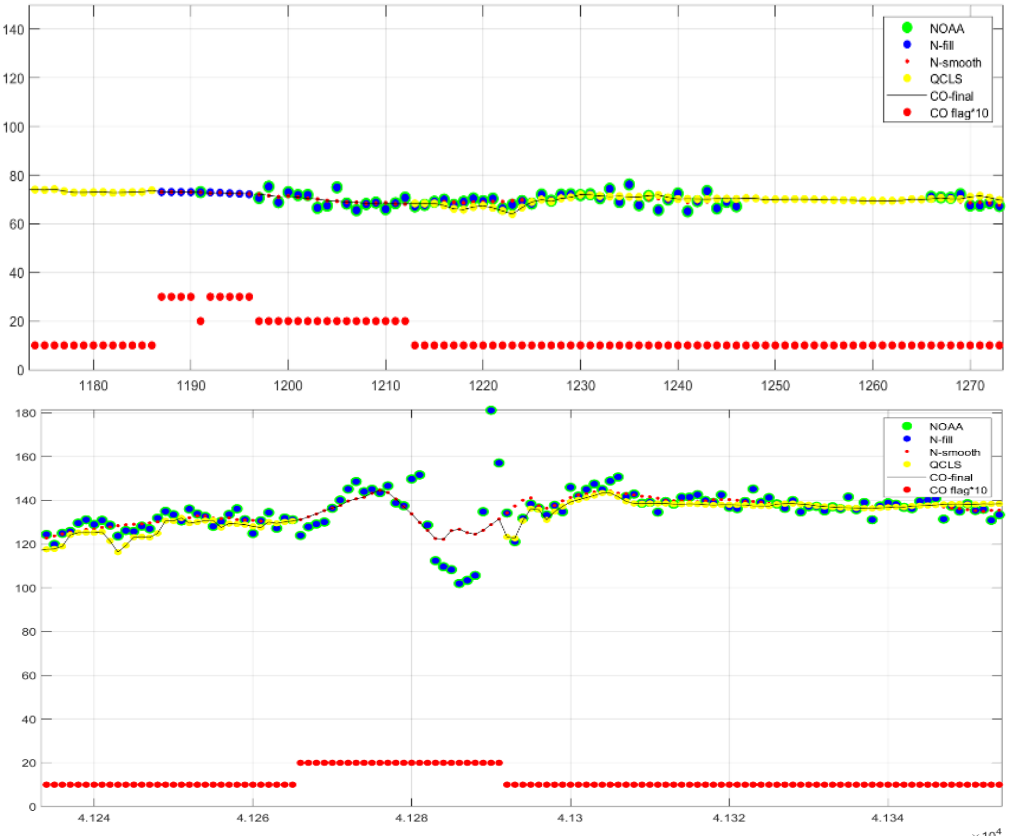

Fig. S3. Example of CO time series showing all the intermediate CO products and flags. See legend and text.

431

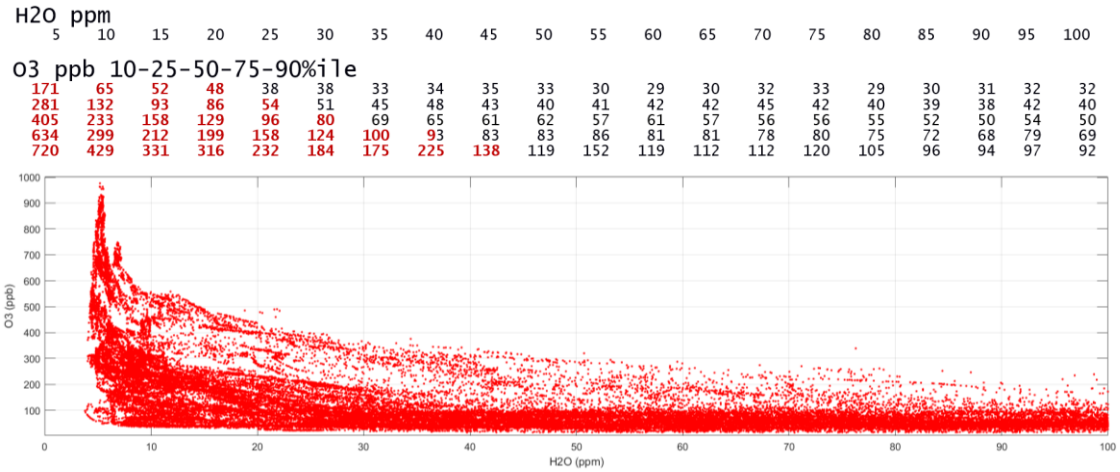

Fig. S4a. Scatter plot of O_3 (ppb) and H_2O (ppm) for all ATom deployments, filtered by H_2O < 100 ppm. The percentiles (10–25–50–75–90 %ile) of O_3 in each 5-ppm-wide bin starting at 5 ppm (= 2.5–7.5 ppm) ending at 100 pm in in the table at the top of this Fig.. Stratospheric influence (red) is clearly seen in the median for < 30 ppm.

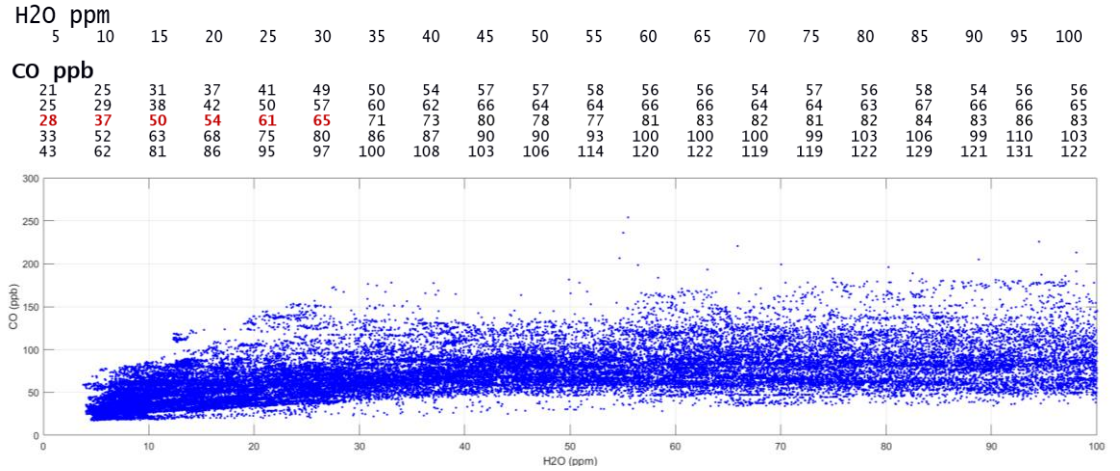

Fig. S4b. Scatter plot of CO (ppb) and H_2O (ppm) for all ATom deployments, filtered by H_2O < 100 ppm. See Fig. S4a.

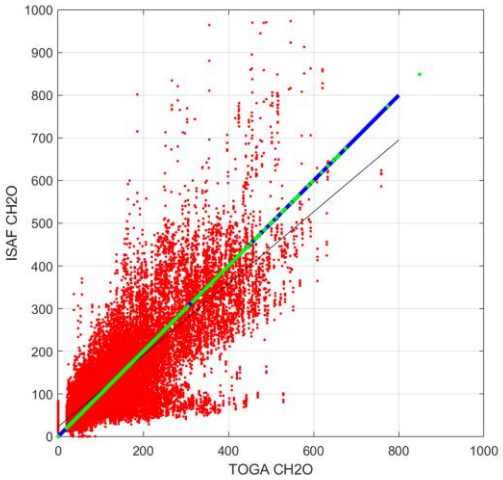

Fig. S5. Scatter plot of coincident HCHO measurements (ppb) from ISAF and TOGA for all ATom deployments. The thick blue-green line is the 1:1 relationship and the thin black line shows a linear regression of ISAF vs. TOGA. Notably, ISAF has more frequent high values > 600 ppb, with some above 1000 ppb (not shown).

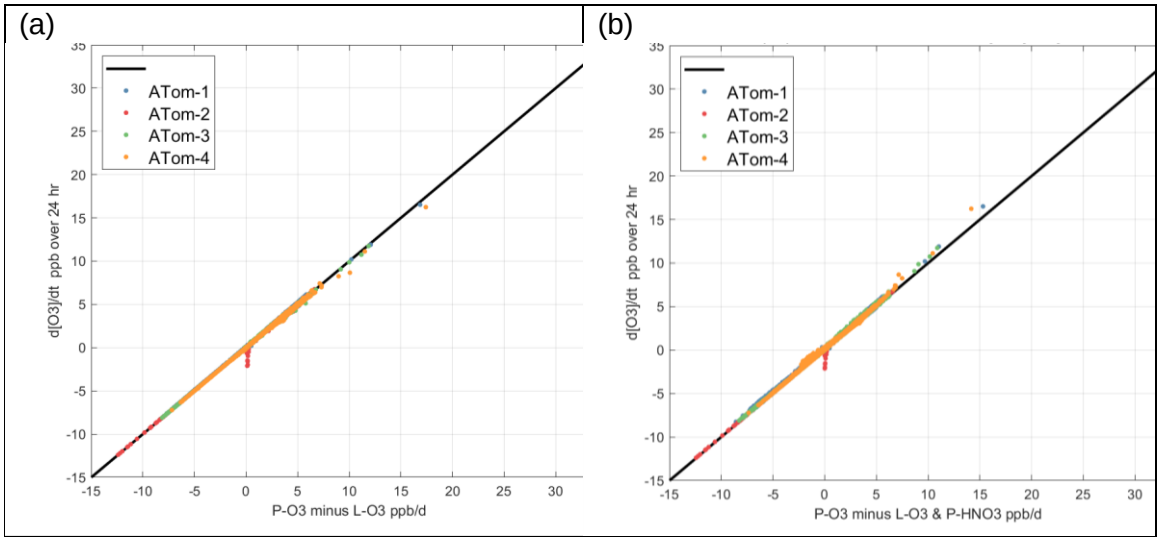

Fig. S6(a) The O_3 tendency d[O_3]/dt over the 24 h integration of reactivities versus the P-O3 minus L-O3 (ppb/d) diagnosed from a few key rates. Results are shown for the four ATom deployments and use the CTM calculations for the third day of the five used to calculate the mean reactivities. Only the ocean basins, 53° S–60° N, are included (about 60 % of all MDS parcels). Some rates affecting odd oxygen are not included in the P-O3 and L-O3, and thus the error in our net O_3 reactivities is P minus L minus d[O_3]/dt. The mean error is very small, -0.01 ppb/d with a root-mean-squared error of 0.04 ppb/d, convincing us that we have accurately diagnosed the P-O3 and L-O3 terms. As an example of missing rates, the production of HNO_3 involves loss of NO_2, which could be seen as a loss of odd-oxygen. Thus in **(b)**, the P-O3 minus L-O3 is augmented by subtracting P-HNO3. In this case we see a shift of the points to slightly above the 1:1 line, indicating that odd-nitrogen driven loss of O_3 is likely the explanation. The few but very obvious red points (ATom-2) below the 1:1 line at P minus L ~ 0 do not shift like the others and investigation shows they are marine boundary layer parcels with extremely large hydrocarbon and NOx abundances, possibly a ship plume.

455

Table S1. ATom flight data

ATom research flights in the Mor.2020-05-27…tbl (149,133 parcels)							Airport removed (146,494 parcels)	
ATom deployment	Research Flight no.	ATom flight	Airports	parcel begin	parcel end	YYYYMMDD	parcel begin	parcel end
1	1	1	PMD PMD*	1	3380	20160729	1	3333
1	2	2	PMD ANC	3381	7038	20160801	3334	6939
1	3	3	ANC KOA	7039	9658	20160803	6940	9526
1	4	4	KOA PPG	9659	12760	20160806	9527	12583
1	5	5	PPG CHC	12761	15141	20160808	12584	14917
1	6	6	CHC PUQ	15142	18976	20160812	14918	18692
1	7	7	PUQ ASI	18977	22355	20160815	18693	21998
1	8	8	ASI TER	22356	25431	20160817	21999	25040
1	9	9	TER SFJ	25432	28976	20160820	25041	28544
1	10	10	SFJ MSP	28977	31127	20160822	28545	30663
1	11	11	MSP PMD	31128	32899	20160823	30664	32383
2	1	12	PMD PMD*	32900	36621	20170126	32384	36061
2	2	13	PMD ANC	36622	40115	20170129	36062	39480
2	3	14	ANC KOA	40116	43062	20170201	39481	42360
2	4	15	KOA NAN	43063	46470	20170203	42361	45717
2	5	16	NAN CHC	46471	49562	20170205	45718	48774
2	6	17	CHC PUQ	49563	53116	20170210	48775	52267
2	7	18	PUQ ASI	53117	56358	20170213	52268	55390
2	8	19	ASI TER	56359	59468	20170215	55391	58446
2	9	20	TER THU	59469	62151	20170218	58447	61088
2	10	21	THU ANC	62152	64893	20170219	61089	63762
2	11	22	ANC PMD	64894	66978	20170221	63763	65807
3	1	23	PMD PMD*	66979	70683	20170928	65808	69465
3	2	24	PMD ANC	70684	74281	20171001	69466	73001
3	3	25	ANC KOA	74282	76949	20171004	73002	75608
3	4	26	KOA NAN	76950	80163	20171006	75609	78754
3	5	27	NAN CHC	80164	83472	20171008	78755	82000
3	6	28	CHC PUQ	83473	87028	20171011	82001	85462
3	7	29	PUQ PUQ^	87029	90872	20171014	85463	89225
3	8	30	PUQ ASI	90873	94279	20171017	89226	92576
3	9	31	ASI SID	94280	95928	20171019	92577	94191
3	10	32	SID TER	95929	98695	20171020	94192	96916
3	11	33	TER BGR	98696	102094	20171023	96917	100272
3	12	34	BGR ANC	102095	105540	20171025	100273	103677
3	13	35	ANC PMD	105541	107873	20171027	103678	105983
4	1	36	PMD PMD*	107874	111294	20180424	105984	109357
4	2	37	PMD ANC	111295	115012	20180427	109358	113028
4	3	38	ANC KOA	115013	117934	20180429	113029	115847
4	4	39	KOA NAN	117935	120880	20180501	115848	118741
4	5	40	NAN CHC	120881	123717	20180503	118742	121542
4	6	41	CHC PUQ	123718	127370	20180506	121543	125122
4	7	42	PUQ PUQ^	127371	131238	20180509	125123	128934
4	8	43	PUQ REC	131239	134829	20180512	128935	132463
4	9	44	REC TER	134830	138214	20180514	132464	135770
4	10	45	TER SFJ	138215	141697	20180517	135771	139210
4	11	46	SFJ BGR	141698	142846	20180518	139211	140316
4	12	47	BGR ANC	142847	146670	20180519	140317	144095
4	13	48	ANC PMD	146671	149133	20180521	144096	146494

* 4 flights to equator following 120W. ^ 2 flights to 80S and 86S over Antarctica.

456

457

Table S2. MDS data and source

id#	MDS data designation	Description	ATom source name
1	parcel_M	Unique sequential parcel number for all MDS 10s data, beginning 1,000,001	
2	ATno	ATom deployment number (1:4)	A.no
3	RFno	Research Flight number (1:11, 1:11, 1:13, 1:13)	RF
4	RRno	RF number across all of ATom (1:48)	
5	YYYMMDD	Date (UT) of the start of each RF	YYYYMMDD
6	UTC_M	Start time in sec relative to Date for each 10s parcel	UTC_Start
7	Lat_M	Latitude (-90:+90)	G_LAT
8	Lng_M	Longitude (-180:+180)	G_LONG
9	Alt_M	Altitude (m above mean sea level)	G_ALT
10	P_M	Pressure (hPa)	P
11	T_M	Temperture (K)	T
12	H2O_M	water, ppm (all dry air mole fraction)	H2O_DLH
13	RHw_M	relative humidity over liquid water (%)	RHw_DLH
14	O3_M	ozone, ppb	O3_CL
15	CO_M	carbon monoxide, ppb	(1) CO_QCLS, (2) CO_NOAA
16	CH4_M	methane, ppb	(1) CH4_NOAA, (2) CH4_QCLS
17	NOx_M	odd-nitrogen, NO+NO2, ppt	NO_CL + NO2_CL
18	NOxPSS_M	odd-nitrogen, with photo-stationary state NO2, ppt	NOx_PSS
19	HNO3_M	nitric acid, HONO2, ppt	HNO3_CIT
20	HNO4_M	pernitric acid, HO2NO2, ppt	PNA_CIT
21	PAN_M	peroxyacetyl nitrate, C2H3NO5 - CH3C(O)OONO2, ppt	(1) PAN_GTCIMS, (2) PAN_PECD*
22	CH2O_M	formaldehyde, HCHO, ppt	(1) CH2O_ISAF, (2) CH2O_TOGA
23	H2O2_M	hydrogen peroxide, HOOH, ppt	H2O2_CIT
24	CH3OOH_M	methyl hydrogen peroxide, ppt	MHP_CIT
25	Acetone_M	acetone, CH3C(O)CH3, ppt	Acetone_TOGA
26	Acetald_M	acetaldehyde, CH3C(O)H, ppt	CH3CHO_TOGA
27	C2H6_M	ethane, C2H6, ppt	Ethane_WAS
28	C3H8_M	propane, C3H8, ppt	(1) Propane_WAS, (2) Propane_TOGA
29	iC4H10_M	iso-butane, iC4H10, ppt	(1) iButane_WAS, (2) iButane_TOGA
30	nC4H10_M	n-butane, nC4H10, ppt	(1) nButane_WAS, (2) nButane_TOGA
31	Alkanes_M	pentane (C5H12) and higher, ppt	iPentane_WAS + nPentane_WAS + nHexane_WAS + nHeptane_WAS + x2MePentane_WAS + x3MePentane_WAS
32	C2H4_M	ethene, C2H4, ppt	Ethene_WAS
33	Alkenes_M	propene (C3H6) and higher, ppt	Propene_WAS
34	C2H2_M	acetylene (ethyne), C2H2, ppt	Ethyne_WAS
35	C5H8_M	isoprene, C5H8, ppt	(1) Isoprene_TOGA, (2) Isoprene_WAS
36	Benzene_M	benzene, C6H6, ppt	(1) Benzene_TOGA, (2) Benzene_WAS*

37	Toluene_M	methylbenzene, C7H8, ppt	(1) Toluene_TOGA+EthBenzene_TOGA, (2) Toluene_WAS + EthBenzene_WAS
38	Xylene_M	dimethylbenzene, C8H10, ppt	(1) mpXylene_TOGA+oXylene_TOGA, (2) mpXylene_WAS+oXylene_WAS
39	MeONO2_M	methyl nitrate, CH3ONO2, ppt	MeONO2_WAS
40	EtONO2_M	ethyl nitrate, CH3ONO2, ppt	EthONO2_WAS
41	RONO2_M	higher organo nitrates, R=C3+, ppt	iPropONO2_WAS + nPropONO2_WAS + x2ButONO2_WAS + x3PentONO2_WAS + x2PentONO2_WAS + x3Me2ButONO2_WAS
42	MeOH_M	methanol, CH3OH, ppt	CH3OH_TOGA
43	HCN_M	hydrogen cyanide, ppt	(1) HCN_CIT, (2) HCN_TOGA
44	CH3CN_M	acetonitrile (methyl cyanide), CH3CN, ppt	CH3CN_TOGA
45	SF6_M	sulfure hexafluoride, ppt	(1) SF6_PECD, (2) SF6_UCATS
46	S_nuc_M	particle surface area (um^2/cm^3), nucleation: 0.0027 < Dp <= 0.012 um	S_nucl_AMP
47	S_atk_M	particle surface area (um^2/cm^3), Aitken: 0.012 < Dp <=0.06 um	S_aitken_AMP
48	S_acc_M	particle surface area (um^2/cm^3), accumulation: 0.06 < Dp <=0.50 um	S_accum_AMP
49	S_crs_M	particle surface area (um^2/cm^3), coarse: 0.50 < Dp <=4.8 um	S_coarse_AMP
50	CloudInd_M	cloud indicator (0:4), dimensionless	cloudindicator_CAPS
Note: The flag value, flag_M(:,1:50) is indexed to the 50 variables above. Only flag_M(:,10:50) have meaningful values. The flag values are: 0 (NaNs, only in research flight 46), 1 (primary data), 2 (secondary data), 3 (short-gap interpolation), 4 (long-gap interpolation for troposphere), 5 (missing flight filled) and 6 (long-gap interpolation for stratosphere) are described in text.			

458

459

Table S3a. ATom-1, % of non-NaNs after short-gap interpolation											
RRno	**1**	**2**	**3**	**4**	**5**	**6**	**7**	**8**	**9**	**10**	**11**
<Lat> (deg)	20	62	42	4	-34	-58	-32	18	65	55	38
<Lng> (deg)	-120	-133	-158	-169	-83	-87	-37	-21	-49	-78	-104
<Alt> (m)	7055	8092	7118	6143	6634	7034	6761	6494	6930	6090	7736
# parcels	**3333**	**3606**	**2587**	**3057**	**2334**	**3775**	**3306**	**3042**	**3504**	**2119**	**1720**
H2O_M	100%	100%	100%	100%	100%	100%	100%	100%	100%	100%	100%
RHw_M	100%	100%	100%	100%	100%	100%	100%	100%	100%	100%	100%
O3_M	99%	99%	100%	99%	100%	100%	99%	100%	100%	100%	100%
CO_M	100%	100%	100%	100%	100%	100%	100%	100%	100%	100%	100%
CH4_M	54%	95%	95%	94%	86%	93%	94%	92%	95%	95%	93%
NOx_M	90%	94%	91%	84%	91%	85%	96%	98%	89%	95%	94%
NOxPSS_M	94%	91%	91%	86%	88%	28%	67%	95%	88%	95%	92%
HNO3_M	92%	96%	97%	92%	**0%**	95%	95%	97%	96%	97%	97%
HNO4_M	59%	87%	74%	67%	**0%**	90%	85%	67%	88%	73%	66%
PAN_M	78%	67%	48%	90%	40%	87%	97%	93%	98%	92%	95%
CH2O_M	99%	100%	100%	100%	100%	100%	100%	100%	100%	100%	100%
H2O2_M	92%	96%	97%	92%	**0%**	95%	95%	97%	96%	97%	97%
CH3OOH_M	56%	69%	81%	83%	84%	79%	81%	82%	82%	79%	79%
Acetone_M	89%	92%	88%	98%	92%	90%	93%	94%	94%	94%	94%
Acetald_M	89%	92%	88%	98%	90%	90%	90%	94%	93%	94%	94%
C2H6_M	50%	32%	43%	44%	62%	37%	39%	43%	40%	46%	45%
C3H8_M	90%	95%	92%	97%	97%	95%	96%	97%	96%	98%	95%
iC4H10_M	95%	95%	92%	98%	97%	95%	96%	97%	98%	98%	96%
nC4H10_M	95%	95%	92%	98%	97%	95%	96%	97%	98%	98%	96%
Alkanes_M	50%	32%	43%	44%	62%	37%	39%	43%	40%	46%	45%
C2H4_M	50%	32%	43%	44%	62%	37%	39%	43%	40%	46%	45%
Alkenes_M	50%	32%	43%	44%	62%	37%	39%	43%	40%	46%	45%
C2H2_M	50%	32%	43%	44%	62%	37%	39%	43%	40%	46%	45%
C5H8_M	95%	95%	92%	98%	97%	95%	96%	97%	98%	98%	96%
Benzene_M	95%	95%	92%	98%	97%	95%	96%	97%	98%	98%	96%
Toluene_M	100%	99%	94%	98%	98%	99%	100%	99%	100%	100%	99%
Xylene_M	100%	99%	94%	98%	98%	99%	100%	99%	100%	100%	99%
MeONO2_M	50%	32%	43%	44%	55%	37%	39%	43%	33%	43%	43%
EtONO2_M	50%	31%	40%	43%	47%	28%	34%	42%	31%	39%	39%
RONO2_M	50%	32%	43%	44%	62%	37%	39%	43%	40%	46%	45%
MeOH_M	89%	92%	88%	98%	92%	90%	92%	92%	92%	94%	94%
HCN_M	98%	100%	100%	100%	92%	100%	100%	100%	100%	100%	100%
CH3CN_M	89%	92%	88%	98%	92%	90%	93%	94%	94%	94%	91%
SF6_M	90%	88%	98%	92%	91%	80%	96%	79%	99%	90%	84%
S_nuc_M	95%	92%	93%	99%	92%	87%	91%	94%	91%	88%	93%
S_atk_M	95%	92%	93%	99%	92%	87%	91%	94%	91%	88%	93%
S_acc_M	95%	92%	93%	99%	92%	87%	91%	93%	91%	88%	93%
S_crs_M	95%	92%	93%	99%	92%	87%	91%	93%	91%	88%	93%
CloudInd_M	100%	100%	100%	100%	99%	100%	100%	100%	100%	100%	100%

460

461

Table S3b. ATom-2, % of non-NaNs after short-gap interpolation											
RRno	**12**	**13**	**14**	**15**	**16**	**17**	**18**	**19**	**20**	**21**	**22**
<Lat> (deg)	18	55	40	0	-41	-58	-32	15	60	73	45
<Lng> (deg)	-120	-142	-154	-46	138	-89	-37	-28	-38	-129	-135
<Alt> (m)	8477	6915	5726	7514	7233	7629	8835	6832	5869	5553	6969
# parcels	**3678**	**3419**	**2880**	**3357**	**3057**	**3493**	**3123**	**3056**	**2642**	**2674**	**2045**
H2O_M	100%	100%	100%	100%	100%	100%	100%	100%	100%	100%	100%
RHw_M	100%	100%	100%	100%	100%	100%	100%	100%	100%	100%	100%
O3_M	99%	100%	100%	100%	100%	100%	100%	100%	100%	100%	100%
CO_M	100%	100%	100%	100%	100%	100%	100%	100%	100%	100%	100%
CH4_M	100%	100%	100%	99%	98%	99%	100%	100%	100%	99%	100%
NOx_M	85%	89%	100%	95%	82%	82%	87%	80%	82%	100%	96%
NOxPSS_M											
HNO3_M	90%	**0%**	91%	95%	96%	92%	97%	97%	97%	93%	98%
HNO4_M	82%	**0%**	77%	70%	77%	81%	87%	77%	87%	93%	94%
PAN_M	84%	100%	100%	95%	100%	100%	99%	97%	94%	100%	94%
CH2O_M	100%	100%	100%	100%	100%	100%	100%	100%	100%	100%	100%
H2O2_M	90%	**0%**	91%	95%	96%	92%	97%	97%	97%	93%	98%
CH3OOH_M	67%	62%	71%	67%	65%	58%	58%	59%	58%	60%	56%
Acetone_M	91%	92%	85%	97%	96%	93%	95%	96%	89%	91%	94%
Acetald_M	91%	92%	85%	97%	96%	93%	95%	97%	89%	91%	94%
C2H6_M	38%	28%	45%	36%	42%	43%	40%	47%	56%	58%	61%
C3H8_M	95%	88%	81%	94%	94%	93%	87%	87%	87%	58%	88%
iC4H10_M	97%	94%	91%	97%	97%	95%	95%	97%	94%	95%	97%
nC4H10_M	97%	94%	91%	97%	97%	95%	95%	97%	94%	95%	97%
Alkanes_M	38%	28%	45%	36%	42%	43%	40%	47%	56%	58%	61%
C2H4_M	38%	28%	45%	36%	42%	43%	40%	47%	56%	58%	61%
Alkenes_M	38%	28%	45%	36%	42%	43%	40%	47%	56%	58%	61%
C2H2_M	38%	28%	45%	36%	42%	43%	40%	47%	56%	58%	61%
C5H8_M	97%	94%	93%	97%	97%	95%	96%	98%	94%	96%	97%
Benzene_M	97%	94%	93%	97%	97%	95%	96%	98%	94%	96%	97%
Toluene_M	100%	96%	96%	100%	100%	100%	100%	100%	98%	100%	100%
Xylene_M	100%	96%	96%	100%	100%	100%	100%	100%	98%	100%	100%
MeONO2_M	37%	26%	45%	36%	38%	35%	40%	47%	53%	54%	51%
EtONO2_M	37%	26%	45%	36%	38%	35%	40%	47%	52%	54%	50%
RONO2_M	38%	28%	45%	36%	42%	43%	40%	47%	56%	58%	61%
MeOH_M	90%	92%	83%	97%	92%	93%	95%	97%	89%	91%	94%
HCN_M	99%	89%	100%	100%	100%	98%	100%	100%	100%	93%	100%
CH3CN_M	91%	92%	85%	97%	96%	93%	95%	97%	89%	87%	94%
SF6_M	87%	97%	96%	88%	98%	99%	98%	99%	99%	99%	69%
S_nuc_M	86%	81%	98%	95%	85%	95%	85%	98%	75%	89%	91%
S_atk_M	86%	81%	98%	95%	85%	95%	85%	98%	75%	89%	91%
S_acc_M	86%	81%	97%	95%	84%	95%	85%	98%	75%	88%	91%
S_crs_M	86%	81%	97%	95%	84%	95%	85%	98%	75%	88%	91%
CloudInd_M	100%	100%	100%	97%	100%	100%	100%	100%	100%	100%	100%

462

463

Table S3c. ATom-3, % of non-NaNs after short-gap interpolation													
RRno	**23**	**24**	**25**	**26**	**27**	**28**	**29**	**30**	**31**	**32**	**33**	**34**	**35**
<Lat> (deg)	18	55	42	4	-41	-58	-67	-32	4	22	55	67	46
<Lng> (deg)	-121	-141	-158	-14	63	-91	-50	-36	-19	-26	-43	-105	-136
<Alt> (m)	8988	7623	6720	6781	6844	6836	7263	8169	6678	6329	5522	6231	6033
# parcels	**3658**	**3536**	**2607**	**3146**	**3246**	**3462**	**3763**	**3351**	**1615**	**2725**	**3356**	**3405**	**2306**
H2O_M	100%	100%	100%	100%	100%	100%	100%	100%	100%	100%	100%	100%	100%
RHw_M	100%	100%	100%	100%	100%	100%	100%	100%	100%	100%	100%	100%	100%
O3_M	99%	100%	100%	100%	100%	100%	100%	100%	89%	99%	100%	100%	100%
CO_M	100%	100%	100%	100%	100%	100%	100%	100%	100%	100%	100%	100%	100%
CH4_M	100%	98%	100%	100%	100%	100%	100%	100%	100%	100%	100%	100%	100%
NOx_M	**0%**	98%	100%	100%	97%	100%	87%	94%	89%	94%	99%	100%	100%
NOxPSS_M													
HNO3_M	96%	96%	96%	95%	97%	91%	94%	96%	91%	85%	97%	90%	66%
HNO4_M	**0%**	**0%**	**0%**	**0%**	**0%**	**0%**	**0%**	**0%**	**0%**	**0%**	**0%**	**0%**	**0%**
PAN_M	100%	100%	100%	98%	100%	100%	99%	99%	100%	98%	100%	98%	100%
CH2O_M	100%	100%	100%	100%	100%	100%	98%	100%	100%	100%	100%	100%	100%
H2O2_M	96%	96%	96%	95%	97%	91%	94%	96%	91%	85%	97%	90%	95%
CH3OOH_M	61%	59%	59%	60%	58%	58%	59%	61%	58%	53%	67%	60%	64%
Acetone_M	94%	95%	87%	95%	96%	97%	92%	96%	86%	93%	94%	98%	98%
Acetald_M	94%	95%	87%	97%	97%	97%	92%	96%	86%	96%	94%	98%	98%
C2H6_M	46%	47%	61%	57%	52%	48%	33%	33%	36%	33%	40%	39%	50%
C3H8_M	95%	97%	94%	98%	98%	98%	95%	97%	92%	96%	94%	98%	98%
iC4H10_M	95%	97%	94%	99%	98%	98%	95%	97%	91%	96%	94%	98%	98%
nC4H10_M	95%	97%	94%	99%	98%	98%	95%	97%	91%	96%	94%	98%	98%
Alkanes_M	46%	47%	61%	57%	52%	48%	34%	34%	39%	33%	40%	39%	50%
C2H4_M	46%	47%	61%	57%	52%	48%	34%	34%	39%	33%	40%	39%	50%
Alkenes_M	46%	47%	61%	57%	52%	48%	34%	34%	39%	33%	40%	39%	50%
C2H2_M	46%	47%	61%	57%	46%	46%	34%	33%	39%	33%	40%	39%	50%
C5H8_M	95%	97%	94%	99%	98%	98%	95%	97%	92%	96%	94%	98%	98%
Benzene_M	95%	97%	94%	99%	98%	98%	95%	97%	92%	96%	94%	98%	98%
Toluene_M	100%	100%	95%	100%	100%	100%	99%	100%	95%	100%	100%	100%	100%
Xylene_M	100%	100%	95%	100%	100%	100%	99%	100%	95%	100%	100%	100%	100%
MeONO2_M	46%	47%	61%	57%	52%	48%	34%	34%	39%	33%	40%	39%	50%
EtONO2_M	46%	47%	61%	57%	52%	48%	34%	34%	39%	33%	40%	39%	50%
RONO2_M	46%	47%	61%	57%	52%	48%	34%	34%	39%	33%	40%	39%	50%
MeOH_M	94%	95%	87%	97%	97%	97%	92%	96%	86%	96%	94%	98%	98%
HCN_M	100%	99%	100%	100%	100%	100%	100%	100%	100%	100%	100%	100%	100%
CH3CN_M	94%	95%	87%	96%	95%	97%	92%	96%	86%	95%	94%	98%	98%
SF6_M	77%	100%	76%	84%	60%	96%	95%	83%	91%	99%	97%	82%	92%
S_nuc_M	92%	77%	74%	94%	91%	86%	92%	91%	99%	88%	91%	81%	92%
S_atk_M	92%	77%	74%	94%	91%	86%	92%	91%	99%	88%	91%	81%	92%
S_acc_M	92%	77%	67%	94%	91%	86%	91%	91%	99%	88%	91%	81%	91%
S_crs_M	92%	77%	67%	94%	91%	86%	91%	91%	99%	88%	91%	81%	91%
CloudInd_M	98%	100%	100%	100%	100%	100%	100%	100%	100%	100%	100%	99%	100%

464

Table S3d. ATom-4, % of non-NaNs after short-gap interpolation

RRno	**36**	**37**	**38**	**39**	**40**	**41**	**42**	**43**	**44**	**45**	**46**	**47**	**48**
<Lat> (deg)	19	56	42	3	-38	-59	-70	-32	13	60	56	67	46
<Lng> (deg)	-121	-141	-158	-132	10	-93	-59	-41	-27	-37	-62	-105	-135
<Alt> (m)	8278	6678	6123	6419	5922	6843	7197	6672	6729	7019	9678	6759	5935
# parcels	**3374**	**3671**	**2819**	**2894**	**2801**	**3580**	**3812**	**3529**	**3307**	**3440**	**1106**	**3779**	**2399**
H2O_M	100%	100%	100%	100%	100%	100%	100%	100%	100%	100%	100%	100%	100%
RHw_M	100%	100%	100%	100%	100%	100%	100%	100%	100%	100%	100%	100%	100%
O3_M	100%	100%	100%	100%	100%	100%	99%	100%	100%	100%	**0%**	100%	100%
CO_M	100%	100%	100%	100%	100%	100%	100%	100%	100%	100%	100%	100%	100%
CH4_M	100%	100%	100%	100%	100%	100%	100%	100%	100%	100%	100%	100%	100%
NOx_M	62%	77%	93%	84%	99%	100%	89%	100%	100%	99%	100%	100%	100%
NOxPSS_M													
HNO3_M	93%	94%	98%	75%	95%	96%	96%	96%	96%	97%	96%	96%	98%
HNO4_M	**0%**	**0%**	**0%**	**0%**	**0%**	**0%**	**0%**	**0%**	**0%**	**0%**	**0%**	**0%**	**0%**
PAN_M	99%	92%	100%	100%	99%	100%	100%	100%	100%	100%	83%	100%	100%
CH2O_M	100%	82%	100%	100%	98%	100%	98%	98%	98%	96%	**0%**	95%	93%
H2O2_M	94%	94%	98%	75%	95%	96%	96%	96%	96%	97%	96%	96%	98%
CH3OOH_M	43%	59%	59%	59%	**0%**	**0%**	**0%**	**0%**	**0%**	69%	67%	**0%**	**0%**
Acetone_M	96%	98%	98%	88%	98%	96%	98%	98%	98%	97%	**0%**	95%	93%
Acetald_M	96%	87%	97%	88%	92%	91%	94%	97%	93%	89%	**0%**	95%	92%
C2H6_M	26%	35%	40%	40%	46%	34%	31%	28%	31%	29%	**0%**	27%	31%
C3H8_M	96%	99%	99%	94%	100%	97%	98%	98%	98%	97%	**0%**	96%	95%
iC4H10_M	96%	99%	99%	94%	100%	97%	98%	98%	98%	97%	**0%**	96%	95%
nC4H10_M	96%	99%	99%	94%	100%	97%	98%	98%	98%	97%	**0%**	96%	95%
Alkanes_M	26%	35%	42%	43%	46%	34%	33%	28%	31%	29%	**0%**	27%	31%
C2H4_M	26%	35%	42%	43%	46%	34%	33%	28%	31%	29%	**0%**	27%	31%
Alkenes_M	26%	35%	42%	43%	46%	34%	33%	28%	31%	29%	**0%**	27%	31%
C2H2_M	26%	35%	42%	43%	46%	34%	33%	28%	31%	29%	**0%**	27%	31%
C5H8_M	96%	99%	99%	94%	100%	97%	98%	98%	98%	97%	**0%**	96%	95%
Benzene_M	96%	99%	99%	94%	100%	97%	98%	98%	98%	97%	**0%**	96%	95%
Toluene_M	100%	100%	99%	95%	100%	100%	100%	100%	100%	100%	**0%**	100%	100%
Xylene_M	100%	100%	99%	95%	100%	100%	100%	100%	100%	100%	**0%**	100%	100%
MeONO2_M	26%	35%	42%	43%	46%	34%	33%	28%	31%	29%	**0%**	27%	31%
EtONO2_M	26%	35%	42%	43%	46%	34%	33%	28%	31%	29%	**0%**	27%	31%
RONO2_M	26%	35%	42%	43%	46%	34%	33%	28%	31%	29%	**0%**	27%	31%
MeOH_M	96%	98%	98%	88%	98%	96%	98%	98%	98%	97%	**0%**	95%	93%
HCN_M	99%	100%	100%	95%	99%	100%	100%	99%	99%	100%	96%	100%	100%
CH3CN_M	96%	98%	98%	88%	98%	96%	98%	98%	98%	97%	**0%**	95%	93%
SF6_M	76%	92%	97%	95%	97%	85%	90%	98%	88%	85%	94%	97%	94%
S_nuc_M	94%	99%	89%	94%	96%	82%	81%	96%	98%	65%	85%	93%	94%
S_atk_M	94%	99%	89%	94%	96%	82%	81%	96%	98%	65%	85%	93%	94%
S_acc_M	94%	99%	88%	94%	96%	82%	81%	95%	98%	65%	85%	92%	94%
S_crs_M	94%	99%	88%	94%	96%	82%	81%	95%	98%	65%	85%	92%	94%
CloudInd_M	100%	100%	100%	100%	100%	100%	99%	94%	100%	100%	100%	100%	99%

467

Table S4. ATom, % of records by flag							
Flags	**0***	**1**	**2**	**3**	**4**	**5**	**6**
H2O_M	0.8%	99.0%	0.0%	0.3%	0.0%	0.0%	0.0%
RHw_M	0.8%	99.0%	0.0%	0.3%	0.0%	0.0%	0.0%
O3_M	0.8%	98.6%	0.0%	0.3%	0.3%	0.0%	0.0%
CO_M	0.8%	79.4%	19.4%	0.1%	0.5%	0.0%	0.0%
CH4_M	0.8%	93.5%	1.3%	1.9%	2.5%	0.0%	0.0%
NOx_M	0.8%	80.8%	0.0%	8.3%	7.6%	2.5%	0.0%
NOxPSS_M	0.8%	82.4%	0.0%	11.8%	5.1%	0.0%	0.0%
HNO3_M	0.8%	78.0%	0.0%	11.6%	5.7%	3.9%	0.0%
HNO4_M	0.8%	28.5%	0.0%	4.0%	8.5%	58.3%	0.0%
PAN_M	0.8%	58.0%	28.4%	7.5%	5.4%	0.0%	0.0%
CH2O_M	0.8%	82.9%	14.9%	0.3%	1.1%	0.0%	0.0%
H2O2_M	0.8%	78.5%	0.0%	11.6%	5.3%	3.9%	0.0%
CH3OOH_M	0.8%	42.0%	0.0%	12.0%	29.4%	15.8%	0.0%
Acetone_M	0.8%	31.7%	0.0%	61.6%	6.0%	0.0%	0.0%
Acetald_M	0.8%	31.4%	0.0%	60.9%	6.9%	0.0%	0.0%
C2H6_M	0.8%	28.0%	0.0%	12.4%	56.3%	0.0%	2.5%
C3H8_M	0.8%	28.0%	53.1%	12.5%	5.1%	0.0%	0.7%
iC4H10_M	0.8%	28.1%	54.9%	12.5%	3.2%	0.0%	0.5%
nC4H10_M	0.8%	28.1%	54.9%	12.5%	3.2%	0.0%	0.5%
Alkanes_M	0.8%	28.1%	0.0%	12.5%	56.0%	0.0%	2.6%
C2H4_M	0.8%	28.1%	0.0%	12.5%	56.0%	0.0%	2.6%
Alkenes_M	0.8%	28.1%	0.0%	12.5%	56.0%	0.0%	2.6%
C2H2_M	0.8%	28.0%	0.0%	12.5%	56.2%	0.0%	2.6%
C5H8_M	0.8%	31.8%	2.3%	61.7%	3.1%	0.0%	0.5%
Benzene_M	0.8%	31.8%	2.3%	61.7%	3.1%	0.0%	0.5%
Toluene_M	0.8%	33.0%	0.6%	64.8%	0.6%	0.0%	0.2%
Xylene_M	0.8%	33.0%	0.6%	64.8%	0.6%	0.0%	0.2%
MeONO2_M	0.8%	27.4%	0.0%	12.3%	57.0%	0.0%	2.6%
EtONO2_M	0.8%	26.8%	0.0%	12.1%	57.8%	0.0%	2.6%
RONO2_M	0.8%	28.1%	0.0%	12.5%	56.0%	0.0%	2.6%
MeOH_M	0.8%	31.7%	0.0%	61.5%	6.0%	0.0%	0.0%
HCN_M	0.8%	78.5%	8.3%	11.6%	0.8%	0.0%	0.0%
CH3CN_M	0.8%	31.7%	0.0%	61.5%	6.0%	0.0%	0.0%
SF6_M	0.8%	10.4%	5.8%	79.2%	3.8%	0.0%	0.0%
S_nuc_M	0.8%	84.6%	0.0%	4.4%	10.3%	0.0%	0.0%
S_atk_M	0.8%	84.6%	0.0%	4.4%	10.3%	0.0%	0.0%
S_acc_M	0.8%	84.1%	0.0%	4.6%	10.6%	0.0%	0.0%
S_crs_M	0.8%	84.1%	0.0%	4.6%	10.6%	0.0%	0.0%
CloudInd_M	0.8%	98.7%	0.0%	0.2%	0.3%	0.0%	0.0%
* The 0.8% flag=0 corresponds to the short flight RF #46, for which we NaN'd all chemical data.							

468

469

Table S5. Test of long-gap interpolation method				
Species	All parcels	Long-gap interpolated parcels		Short-gap fill
(ppt unless noted)	mean	bias (% of mean)	RMSE (% of mean)	RMSE (% of mean)
H2O_M (ppm)	336			16%
RHw_M (%)	40			12%
O3_M (ppb)	80	3%	12%	6%
CO_M (ppb)	80	1%	8%	3%
CH4_M (ppb)	1850	<1%	<1%	<1%
NOx_M	64	-8%	44%	22%
NOxPSS_M	46	-17%	70%	25%
HNO3_M	162	-6%	22%	12%
HNO4_M	26	-7%	54%	28%
PAN_M	87	6%	25%	14%
CH2O_M	140	6%	22%	11%
H2O2_M	250	9%	30%	16%
CH3OOH_M	381	12%	45%	21%
Acetone_M	351	3%	18%	
Acetald_M	56	3%	19%	
C2H6_M	644	2%	16%	
C3H8_M	109	3%	16%	
iC4H10_M	11	6%	29%	
nC4H10_M	21	5%	29%	
Alkanes_M	16	3%	33%	
C2H4_M	6	28%	94%	
Alkenes_M	0.2	17%	78%	
C2H2_M	97	10%	42%	
C5H8_M	0.5	16%	70%	
Benzene_M	15	-12%	33%	
Toluene_M	1	4%	28%	
Xylene_M	0.1	33%	97%	
MeONO2_M	9	-11%	29%	
EtONO2_M	2	-11%	33%	
RONO2_M	5	-5%	37%	
MeOH_M	590	3%	38%	
HCN_M	185	5%	31%	10%
CH3CN_M	114	11%	44%	
SF6_M	9	<1%	1%	<1%

470

471

Table S6. Test of missing flight data

Missing data (ppt unless noted)	All parcels Mean (ppt)	Interpolated RMSE (% of mean)	Flights used
ATom-1 RF-5			
H2O2_M	392	24%	AT-1 RF4, AT-2/3/4 RF-4/5
HNO3_M	139	58%	AT-1 RF4, AT-2/3/4 RF-4/5
HNO4_M	30.2	66%	AT-1 RF4, AT-2 RF-4/5
ATom-2 RF-2			
H2O2_M	125	23%	AT-2 RF-3, AT-1/3/4 RF-2/3
HNO3_M	30.9	52%	AT-2 RF-3, AT-1/3/4 RF-2/3
HNO4_M	14.3	63%	AT-2 RF-3, AT-1 RF-2/3
ATom-3 RF-1			
NOx_M	80.9	55%	AT-3 RF-2, AT-1/2/4 RF-1/2
ATom-3/4 all			
HNO4_M	26.1	105%	AT-1/2 all
ATom-4 RF-5/6/7/8/9/12/13			
CH3OOH_M	336	72%	AT-1/2 RF-5:11, AT-3 RF-5:13, AT-4 RF-4

Notes: Missing flight data are filled using a multiple linear regression from other flights based on the explanatory variables: pressure, noontime solar zenith angle, and latitude (in that order). RMSE is calculated from the residuals of this fit for the flights used in the regression.

472

473

Table S7. Chemistry models

Used in	ID	Model name	Type	Meteorology	Model Grid	References	Point of Contact
clim	GFDL	GFDL-AM3	CCM	NCEP (nudged)	C180 x L48	Horowitz et al., 2003; Li et al. 2017	amfiore @ldeo.columbia.edu
clim, MDS-0	GISS	GISS-E2.1	CCM	Daily SSTs, nudged to MERRA	2° x 2.5° x 40L	Rienecker et al.,	lee.murray @rochester.edu
clim, MDS-0	GMI	GMI-CTM	CTM	MERRA	1° x 1.25° x 72L	Strahan et al., 2013; Duncan et al., 2007	Sarah.A.Strode @nasa.gov
clim, MDS-0	GC	GEOS-Chem	CTM	MERRA-2	2° x 2.5° x 72L	Gelaro et al., 2017	lee.murray @rochester.edu
clim, MDS-0	NCAR	CAM4-Chem	CCM	Nudged to MERRA	0.47° x 0.625° x 52L	Tilmes et al., 2016	emmons @ucar.edu
clim, MDS-0 & 2b	UCI	UCI-CTM	CTM	ECMWF IFS Cy38r1	T159N80 x L60	Holmes et al., 2017; Prather 2015	mprather @uci.edu
MDS-0	F0AM	F0AM	box	MDS+scaled ATom Js	N/A	Wolfe et al., 2016	glenn.m.wolfe @nasa.gov

The descriptions of models used in the paper. The first column denotes if the model's August climatology is used ('clim') and also the MDS versions used. F0AM used chemical mechanism MCMv331 plus J-HNO_4 plus $O(^1D)+CH_4$. For the global models see P2017, P2017, and H2018.

474
475
476
477

Table S8. Reactivity statistics and mean J-values for 3 large domains (Global, Pacific, Atlantic)

Table S8a. Average Reactivity: mean, median, mean of top 10 %

		Models using MDS-0								MDS-2b
Value	Region	F0AM	GC	GISS	GMI	NCAR	UCI	U15	U97	UCIZ*
P-O3, mean, ppb/d										
	Global	2.12	2.12	2.57	2.08	2.22	2.38	2.37	2.37	1.23
	Pacific	1.96	2.00	1.99	1.96	2.01	2.17	2.13	2.15	1.11
	Atlantic	1.96	2.12	3.49	2.20	2.44	2.48	2.48	2.49	1.25
P-O3, median, ppb/d										
	Global	1.50	1.69	1.96	1.64	1.80	1.81	1.80	1.80	0.96
	Pacific	1.36	1.67	1.62	1.52	1.67	1.73	1.69	1.71	0.94
	Atlantic	1.83	1.97	3.34	2.09	2.31	2.18	2.18	2.19	1.10
P-O3, mean of top 10%, ppb/d										
	Global	7.48	6.75	7.98	6.60	6.72	8.07	8.07	8.06	4.06
	Pacific	6.65	5.53	5.55	5.68	5.69	6.54	6.29	6.37	3.03
	Atlantic	4.73	5.32	8.23	5.63	5.88	6.74	6.76	6.84	3.38
L-O3, mean, ppb/d										
	Global	1.81	1.63	1.93	1.70	1.76	1.76	1.74	1.75	1.61
	Pacific	1.65	1.51	1.79	1.55	1.52	1.58	1.53	1.56	1.42
	Atlantic	2.15	2.02	2.37	2.17	2.47	2.28	2.28	2.30	2.12
L-O3, median, ppb/d										
	Global	1.03	0.98	1.23	0.97	1.08	1.03	1.03	1.02	0.94
	Pacific	1.09	1.06	1.31	1.08	1.10	1.10	1.14	1.11	1.02
	Atlantic	1.27	1.20	1.44	1.23	1.60	1.29	1.29	1.29	1.18
L-O3, mean of top 10%, ppb/d										
	Global	6.27	5.70	6.39	5.97	6.36	6.31	6.32	6.33	5.79
	Pacific	5.48	4.78	5.22	4.93	4.77	5.01	4.83	4.96	4.53
	Atlantic	6.05	6.05	6.80	6.40	8.36	6.85	6.88	6.93	6.12
L-CH4, mean, ppb/d										
	Global	0.81	0.76	0.43	0.75	0.73	0.79	0.78	0.78	0.61
	Pacific	0.85	0.82	0.40	0.80	0.79	0.82	0.80	0.81	0.63
	Atlantic	0.80	0.78	0.51	0.81	0.86	0.85	0.85	0.85	0.69
L-CH4, median, ppb/d										
	Global	0.46	0.50	0.37	0.45	0.47	0.48	0.48	0.48	0.40
	Pacific	0.52	0.61	0.36	0.56	0.53	0.59	0.59	0.60	0.50
	Atlantic	0.53	0.57	0.51	0.54	0.66	0.58	0.57	0.56	0.48
L-CH4, mean of top 10%, ppb/d										
	Global	2.67	2.27	1.14	2.31	2.24	2.51	2.49	2.51	1.83
	Pacific	2.71	2.29	1.02	2.34	2.24	2.41	2.32	2.37	1.71
	Atlantic	2.15	1.95	1.08	2.09	2.32	2.26	2.25	2.30	1.74

Table S8b. Percent of total Reactivity in the top 50 %, top 10 %, top 3 % of parcels

		Models using MDS-0								MDS-2b
Value	Region	F0AM	GC	GISS	GMI	NCAR	UCI	U15	U97	UCIZ*
P-O3, % of total R in top 50%										
	Global	83%	82%	82%	83%	82%	83%	83%	83%	84%
	Pacific	84%	80%	77%	81%	80%	81%	81%	81%	80%
	Atlantic	76%	79%	76%	78%	77%	79%	79%	79%	83%
P-O3, %of total R in top 10%										
	Global	35%	32%	31%	32%	30%	34%	34%	34%	33%
	Pacific	34%	28%	28%	29%	29%	30%	30%	30%	27%
	Atlantic	24%	25%	24%	26%	24%	27%	27%	28%	27%
P-O3, %of total R in top 3%										
	Global	16%	11%	12%	12%	12%	13%	12%	13%	12%
	Pacific	10%	10%	9%	10%	9%	12%	12%	12%	10%
	Atlantic	14%	13%	13%	13%	16%	14%	14%	14%	14%
L-O3, % of total R in top 50%										
	Global	88%	88%	86%	88%	87%	88%	88%	88%	88%
	Pacific	88%	86%	85%	86%	85%	86%	85%	86%	85%
	Atlantic	87%	87%	86%	88%	87%	88%	88%	88%	88%
L-O3, %of total R in top 10%										
	Global	35%	35%	33%	35%	36%	36%	36%	36%	36%
	Pacific	33%	32%	29%	32%	31%	32%	32%	32%	32%
	Atlantic	28%	30%	29%	30%	34%	30%	30%	30%	29%
L-O3, %of total R in top 3%										
	Global	14%	13%	13%	13%	16%	14%	14%	14%	14%
	Pacific	14%	13%	12%	13%	13%	13%	13%	13%	14%
	Atlantic	10%	11%	11%	10%	16%	11%	11%	11%	11%
L-CH4, % of total R in top 50%										
	Global	89%	88%	80%	89%	87%	89%	89%	89%	87%
	Pacific	89%	87%	78%	88%	86%	87%	87%	87%	84%
	Atlantic	85%	84%	74%	86%	84%	86%	86%	86%	85%
L-CH4, %of total R in top 10%										
	Global	33%	30%	27%	31%	31%	32%	32%	32%	30%
	Pacific	32%	28%	26%	29%	29%	29%	29%	29%	27%
	Atlantic	27%	25%	21%	26%	27%	27%	27%	27%	25%
L-CH4, %of total R in top 3%										
	Global	14%	11%	11%	11%	11%	12%	12%	12%	11%
	Pacific	14%	10%	10%	11%	10%	12%	11%	12%	10%
	Atlantic	10%	8%	7%	9%	10%	10%	9%	10%	9%

484

Table S8c. Mean J-values

		models								
Value	Region	F0AM	GC	GISS	GMI	NCAR	UCI	U15	U97	UCIZ
J-O1D, mean, e-5 /s										
	Global	1.29	1.12	1.64	1.20	1.29	1.17	1.17	1.17	1.16
	Pacific	1.38	1.26	1.85	1.33	1.38	1.30	1.29	1.30	1.30
	Atlantic	1.32	1.17	1.61	1.26	1.46	1.26	1.26	1.27	1.25
J-NO2, mean, e-3 /s										
	Global	4.55	4.33	5.36	4.30	4.51	4.75	4.72	4.73	4.66
	Pacific	4.50	4.43	5.47	4.38	4.60	4.86	4.79	4.84	4.82
	Atlantic	4.54	4.39	5.15	4.37	4.59	4.91	4.90	4.93	4.77

485
486 Global includes all ATom-1 parcels, Pacific considers all measurements over the Pacific Ocean from 53°S to
487 60°N, and Atlantic uses parcels from 53° S to 60° N over the Atlantic Ocean. All parcels are weighted
488 inversely by the number of parcels in each 10° latitude by 100 hPa bin, and by cosine(latitude). Results
489 from MDS-0 are shown because we have results from six models. Results from the updated MDS-2b are
490 shown (UCIZ*) using the using the current UCI CTM model UCIZ and the RDS* protocol that preprocesses
491 the MDS-2b initializations with a 24 h decay of HNO4 and PAN according to their local thermal
492 decomposition frequencies, see text.
493
494

495

Table S9. Standard deviation across 5 separated days in August (% of mean reactivity or J-value) using MDS-0.					
	P-O3	L-O3	L-CH4	J-O1D	J-NO2
GC	11%	9%	10%	9%	9%
GISS	22%	14%	17%	14%	12%
GMI	10%	9%	10%	10%	10%
NCAR	23%	32%	28%	17%	16%
UCI	10%	10%	11%	10%	11%

496
497

SI References

Duncan, B.N., Logan, J.A., Bey, I., Megretskaia, I.A., Yantosca, R.M., Novelli, P.C., Jones, N.B. and Rinsland, C.P., 2007. Global budget of CO, 1988–1997: Source estimates and validation with a global model. Journal of Geophysical Research: Atmospheres, 112(D22).

Gelaro, R., McCarty, W., Suárez, M.J., Todling, R., Molod, A., Takacs, L., Randles, C.A., Darmenov, A., Bosilovich, M.G., Reichle, R. and Wargan, K., 2017. The modern-era retrospective analysis for research and applications, version 2 (MERRA-2). Journal of climate, 30(14), pp.5419-5454.

Holmes, C.D. and Prather, M.J., 2017. An atmospheric definition of the equator and its implications for atmospheric chemistry and climate. Nature Geoscience.

Horowitz, L.W., Walters, S., Mauzerall, D.L., Emmons, L.K., Rasch, P.J., Granier, C., Tie, X., Lamarque, J.F., Schultz, M.G., Tyndall, G.S. and Orlando, J.J., 2003. A global simulation of tropospheric ozone and related tracers: Description and evaluation of MOZART, version 2. Journal of geophysical research: Atmospheres, 108(D24).

Li, D., Zhang, R. and Knutson, T.R., 2017. On the discrepancy between observed and CMIP5 multi-model simulated Barents Sea winter sea ice decline. Nature Communications, 8(1), pp.1-7.

Prather, M.J., Zhu, X., Flynn, C.M., Strode, S.A., Rodriguez, J.M., Steenrod, S.D., Liu, J., Lamarque, J.F., Fiore, A.M., Horowitz, L.W. and Mao, J., 2017. Global atmospheric chemistry–which air matters. Atmospheric Chemistry and Physics, 17(14), pp.9081-9102.

Prather, M.J., Flynn, C.M., Zhu, X., Steenrod, S.D., Strode, S.A., Fiore, A.M., Correa, G., Murray, L.T. and Lamarque, J.F., 2018. How well can global chemistry models calculate the reactivity of short-lived greenhouse gases in the remote troposphere, knowing the chemical composition. Atmospheric Measurement Techniques, 11(5), pp.2653-2668.

Rienecker, M.M., Suarez, M.J., Gelaro, R., Todling, R., Bacmeister, J., Liu, E., Bosilovich, M.G., Schubert, S.D., Takacs, L., Kim, G.K. and Bloom, S., 2011. MERRA: NASA's modern-era retrospective analysis for research and applications. Journal of climate, 24(14), pp.3624-3648.

Strahan, S.E., Douglass, A.R. and Steenrod, S.D., 2016. Chemical and dynamical impacts of stratospheric sudden warmings on Arctic ozone variability. Journal of Geophysical Research: Atmospheres, 121(19), pp.11-836.

Tilmes, S., Sanderson, B.M. and O'Neill, B.C., 2016. Climate impacts of geoengineering in a delayed mitigation scenario. Geophysical Research Letters, 43(15), pp.8222-8229.

Wofsy, S.C., Afshar, S., Allen, H.M., Apel, E.C., Asher, E.C., Barletta, B., Bent, J., Bian, H., Biggs, B.C., Blake, D.R. and Blake, N., 2018. ATom: Merged atmospheric chemistry, trace gases, and aerosols. ORNL DAAC Oak Ridge, Tennessee, USA.

Wolfe, G.M., Marvin, M.R., Roberts, S.J., Travis, K.R. and Liao, J., 2016. The framework for 0-D atmospheric modeling (F0AM) v3. 1. Geoscientific Model Development, 9(9), pp.3309-3319.